Study of Dieless Radial Spinning for Thick-Walled Cylindrical Parts With External Grooves

Famei Liu
  State Key Laboratory of Materials Processing and Die & Mould Technology, Huazhong University of Science and Technology, No. 1037 Luoyu Road, Wuhan 430074, Hubei, China

Junsong Jin (✉ kingboster@tom.com)
  Huazhong University of Science and Technology

Wei Rao
  State Key Laboratory of Materials Processing and Die & Mould Technology, Huazhong University of Science and Technology, No. 1037 Luoyu Road, Wuhan 430074, Hubei, China

Ying Wang
  State Key Laboratory of Materials Processing and Die & Mould Technology, Huazhong University of Science and Technology, No. 1037 Luoyu Road, Wuhan 430074, Hubei, China

Chang Gao
  State Key Laboratory of Materials Processing and Die & Mould Technology, Huazhong University of Science and Technology, No. 1037 Luoyu Road, Wuhan 430074, Hubei, China

Xuefeng Tang
  State Key Laboratory of Materials Processing and Die & Mould Technology, Huazhong University of Science and Technology, No. 1037 Luoyu Road, Wuhan 430074, Hubei, China

Xinyun Wang
  State Key Laboratory of Materials Processing and Die & Mould Technology, Huazhong University of Science and Technology, No. 1037 Luoyu Road, Wuhan 430074, Hubei, China

Research Article

Study of Dieless Radial Spinning for Thick-Walled Cylindrical Parts with External Grooves

Famei Liu, Junsong Jin[*], Wei Rao, Ying Wang, Chang Gao, Xuefeng Tang, Xinyun Wang

State Key Laboratory of Materials Processing and Die & Mould Technology, Huazhong University of Science and Technology,

No. 1037 Luoyu Road, Wuhan 430074, Hubei, China

Abstract

Thick-walled cylindrical parts with external grooves are common components in the automobile and aviation fields. Such components can be produced by pressing the outer surface of a spinning thick-walled aluminum alloy tube by the dieless radial spinning process. The forming characteristics in the spinning process and the effects of various process parameters on forming were studied by using orthogonal tests and finite element simulations. During the forming process, bulge and thickness reductions occur because of material flow. The results of an investigation of process parameter effects show that the stress yield ratio (ξ) had no significant effect on forming. However, the feed thickness ratio (η) and initial wall thickness of the tube (t_0) crucially affected the forming quality (e.g., the heights of bulges and thickness reduction in the groove area). Thick-walled tubes presented different phenomena compared to the thin-walled.

Keywords Thick-walled; dieless; spinning; orthogonal test; finite element; aluminum alloy

Highlights of the research:

1. The thick-walled cylindrical parts with external grooves were produced by the dieless radial spinning process.

2. The effects of the process parameters on the forming quality were analyzed.

3. The difference between the thick-walled tubes thin-walled tubes while spinning process was revealed.

4. A suggestion about the values of the parameters to obtain an eligible part were given.

1 Introduction

The spinning forming process is a local forming method for producing hollow parts, and is widely used in the aviation, aerospace, military, and automobile industries [1, 2]. As an advanced forming process, spinning process has several significant merits [3]. Less load and energy are acquired for spinning process since the material is locally deformed. The production efficiency is much higher than traditional processes, because fewer working steps are acquired.

---

[*] Corresponding author: Junsong Jin   Email: jsjin@hust.edu.cn.

Besides, it costs fewer metals because of high material utilization. Thus, the spinning process is a kind of green technology. Spinning processes are mainly classified as conventional spinning, shear spinning, and tube spinning [3]. Tube spinning (i.e., flow forming) is a popular process for producing cylindrical tubular components [4, 5]. On the basis of the tube deformation characteristics, tube spinning can be divided into thickness-reducing spinning and diameter-reducing spinning. The diameter-reducing spinning process has been frequently reported and is widely used.

Huang et al. [6] used simulations and experiments to introduce neck-spinning at tube ends (TENS), which released the effects of friction, speed, and the tip radius of the rollers on forming. Zoghi et al. [7] investigated deformation during TENS by analyzing the strain distributions in different layers and axial positions. Xia et al. [8, 9] studied the stress and strain distributions and the dimensional accuracy in different passes, and examined the defects that can occur during TENS of non-axisymmetric offset tubes. Arai [10] proposed a three-dimensional CAD model for calculating the positions at which the roller touches the tube during TENS of a non-axisymmetric offset tube. Yao and Makoto [11] performed experiments on paraxial spinning at one end and identified the forming characteristics.

These processes mentioned above are to reduce the radius of the tube end. Some products, including corrugated pipes, exhaust pipes, and pulleys, require changes to the radius at the middle of the tube. Kwiatkowski et al. [12] used analytical models to develop dieless neck-spinning at the middle of a tube with two principal tool movements. Guo et al. and Yao and Makoto [13, 14] used a paraxial spinning process to prepare a reducer tube and studied the plastic rheology and microstructural variations of the blank. Grzancic et al. [15] manufactured tubes with various cross-sectional geometries by controlling the tool movements and established an analytical model for predicting forming behavior. Zhu et al. [16] compared four typical spinning methods for producing large sheaves and concluded that counter-roller spinning is the best option.

These studies above introduced several spinning processes for changing the radius of a thin-walled tube. However, none of them involved thick-walled tubes. Obviously, the spinning process for the thin-walled tube is classified as sheet forming, while the spinning process for thick-walled tube is classified as bulk forming. Thus, it is valuable to research the thick-walled tubes by spinning process since the metal flow during neck-spinning varies with changes in the tube thickness.

Thick-walled cylindrical parts with annular grooves (e.g., pistons) are widely used in hydraulic and pneumatic transmission systems. The parts are cup shaped and have annular grooves on the outer surface for O-ring seals. The traditional manufacturing method used to ensure groove strength is to machine the annular groove at the outer surface of a cup with a much thicker wall than that of the groove. The material utilization and production efficiency in this traditional method are low. The performance of the part is poor because the integrity of the material flow line is destroyed. The traditional method also increases the weight of the part, which is contrary to the principle of producing lightweight components. If the spinning method is used, the outer groove can be formed from a cup blank of constant thickness. The comparison of material utilization rate between traditional method and spinning process is shown in Fig. 1. Where t_g is the thickness of groove required. t_{0s} and t_{0t} refer to the initial wall thickness of blank by spinning and traditional method respectively. Obviously, t_{0t} is much larger than t_{0s}. Compared with the traditional method, the spinning process has obvious merits, such as high production efficiency, high material utilization, a continuous metal streamline, good mechanical properties, and light weight.
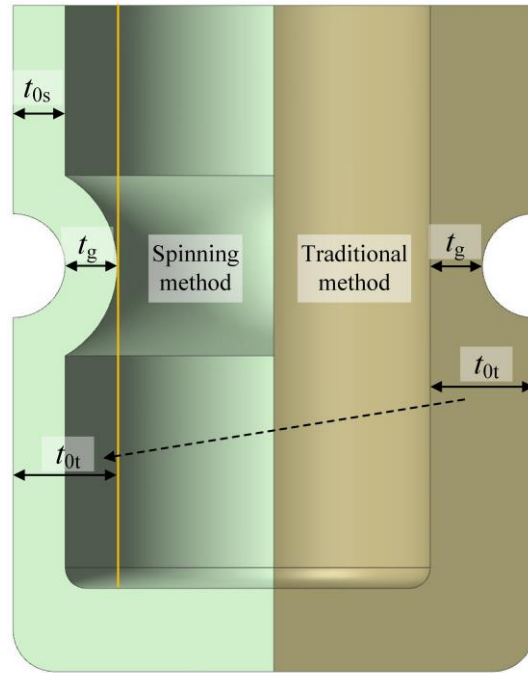
Fig. 1 Comparison of initial thickness between spinning method and traditional method

The two-wheel dieless radial spinning process (DRSP) was proposed for the production of thick-walled cylindrical parts with external grooves. Orthogonal tests and finite element (FE) simulations were used to investigate the deformation characteristics, stress and strain distributions, and effects of various parameters on the forming quality.

2 Materials and method

2.1 Dieless radial spinning process (DRSP)

The principle of the DRSP is shown in Fig. 2(a). First, the upper die presses the cup blank on the lower die with a circular groove at a certain pressure F_Z; the three components are coaxial. The upper and lower dies then rotate at an angular velocity ω, which drives the blank to rotate at the same velocity as that relying on friction. At the same time, two rollers, which are symmetrically distributed on both sides of the blank, start to feed synchronously to the blank axis at a speed v. When the rollers contact the outer surface of the blank, they passively rotate in the opposite direction relative to the blank, driven by friction. Under pressing with the rollers, the material in the contact area of the blank and the roller is plastically deformed and an external groove is generated. The rollers stay for a certain time to finish the groove when they feed to the maximum depth, and then the rollers return to the initial position.
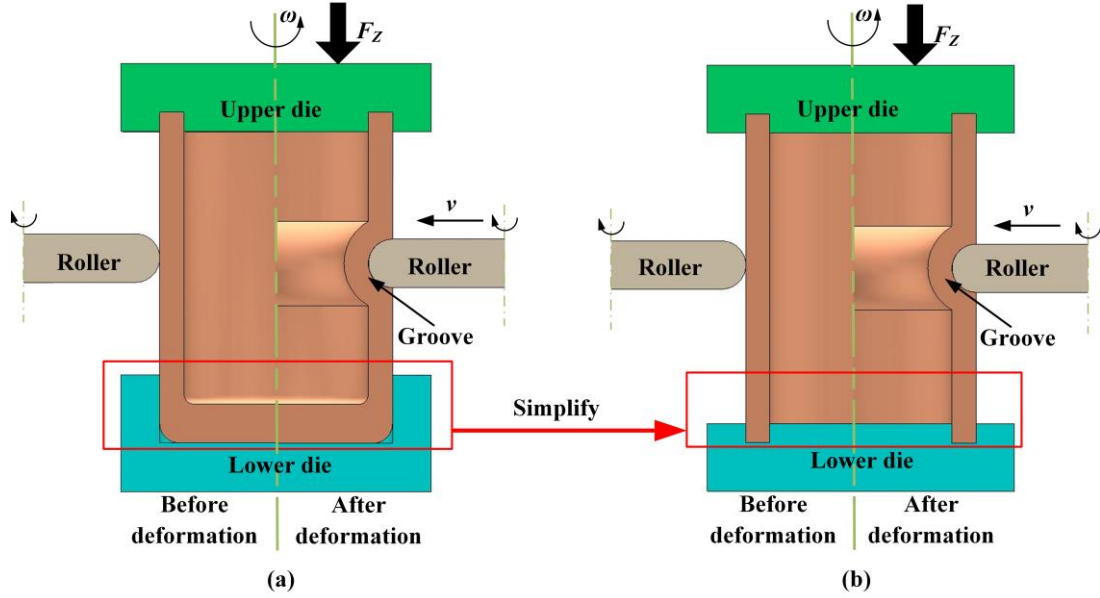
Fig. 2 Schematic diagram of DRSP: (a) original model and (b) simplified model

Deformation is mainly concentrated near the groove, and therefore the effect of the cup bottom on the forming process can be ignored. To reduce the difficulty of making blanks, the experimental blanks were simplified into bottomless cylindrical parts, as shown in Fig. 2(b). The lower die was correspondingly designed as an annular groove consistent with the upper die.

2.2 Materials

The blanks were 6061-T6 aluminum alloy tubes. The dimensions of the initial blank were height 80 mm, inner diameter 30 mm, and wall thickness 8 mm. Blanks with other specifications were produced by turning. The mechanical properties and true stress–strain curve of the blanks are shown in Table 1 and Fig. 3.

Table 1 Main mechanical properties of 6061-T6 aluminum alloy

| Tensile stress	Yield stress	Density	Young's modulus	Poisson's ratio
343MPa	270MPa	2900kg/m^3	68.9GPa	0.33
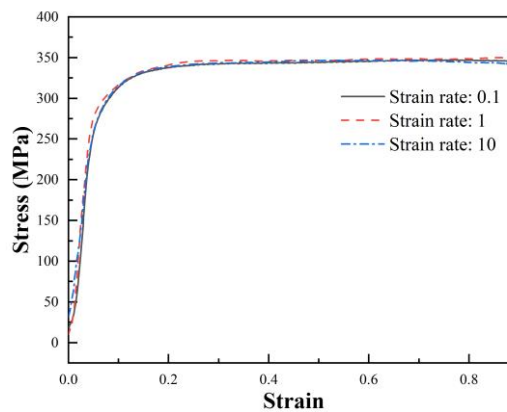
Fig. 3 True stress–strain curve of 6061 aluminum alloy

2.3 Experimental equipment and mold

The equipment used in the experiments in this study was the PS-CNCVGP450 vertical CNC spinning machine (Fig. 4). The rotational speed of the spindle and movement of the rollers in the X, Y, and Z directions were controlled by the CNC system; the control accuracy was 0.01 mm. The pressure of the upper die was controlled by a hydraulic

valve. The diameter of the roller was 180 mm, the thickness was 10 mm, and the side was a semicircle of radius 5 mm.

Fig. 4 PS-CNCVGP450 vertical CNC spinning machine and molds

2.4 Finite element (FE) simulation

In studies of spinning processes, FE simulation is an efficient method for investigation of the deformation characteristics of plastic forming processes and defect prediction [17-20]. The FE software Simufact.forming was used for DRSP simulations and was used in combination with experimental results to analyze and explain the deformation characteristics and parameter effects. The FE model of DRSP is shown in Fig. 5.

The key dimensions of the molds and the blank, and the blank material used in the simulations were consistent with those in the experiments. The upper die, lower die, and rollers were set as rigid bodies. The blank was an elastoplastic deformable model; it was divided by hexahedral elements via the ring-meshing method. The initial element dimensions were 1.2 mm in the axial and radial directions, and 12 mm in the tangential direction. The areas above and below the center face of the blank for 10 mm in the axial direction were locally refined by a refinement box; this improved the simulation accuracy. The re-meshing technique was used during the simulation to avoid element distortion resulting from severe deformation.

The contacts between the blank and the upper die, and the blank and the lower die, were set to be "glued", which means that there was no relative displacement between the contact bodies. The contacts between the blank and the rollers were set to be "touching", which means a relative movement between the contact bodies was possible. The shear friction model was adopted; the friction coefficient was 0.1. The shear friction model was described by the formulation as follows:

$\tau_R = m \cdot k$ with $k = 0.577 \cdot \sigma_V$ (1)

Where τ_R refers to friction stress, m refers to shear friction coefficient, k refers to ultimate shear strength, σ_V is field strength.

During the forming process, the temperatures of the blank, the molds, and the environment were all set at 20 °C. The effect of the deformation temperature was not considered.
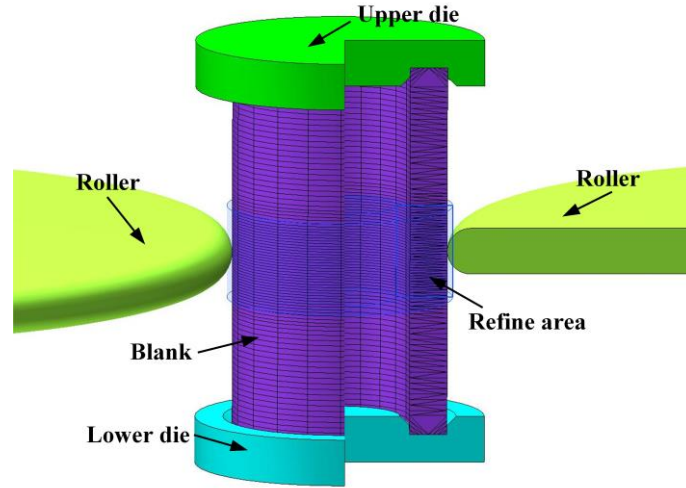
Fig. 5 FE model of DRSP

2.5 Orthogonal tests

Changing the pressure F_Z of the upper die changes the axial stress on the blank. An excessive F_Z causes the blank to collapse, and the blank will slide because of the small frictional force when F_Z is too small. The effect of F_Z is related to the strength of the blank, therefore the stress yield ratio ξ (the ratio of the applied stress to the yield stress) is investigated and defined as

$$\xi = F_Z/(A_S \cdot \sigma_S) \quad (2)$$

where A_s is the cross-sectional area of the blank and σ_s is the yield stress of the blank.

The material flow differs depending on the initial blank thickness t_0. The material flow is similar to that for sheet-metal forming when t_0 is small, but resembles that for volume forming when t_0 is larger. The value of t_0 directly affects the resistance during feeding of the rollers. Experimental results showed that the feeding distance of the roller, m, is an important parameter in the spinning process. The resistance in the tangential direction of the roller increases with increasing m, which affects the stability of the experiment. If m is too small, the outer surface of the groove will be peeled because of repeated grinding over a long period. To exclude the effect of t_0, the feed thickness ratio η (the ratio of the feeding distance per round of the roller to the tube wall thickness) was investigated and defined as

$$\eta = m/t_0 \quad (3)$$

It can be seen from the pre-experiment that when $0.05 < \xi < 0.3$, the blank will not collapse or slide during the forming process; when $\eta > 0.3$, the impact of η on the forming quality is small. The wall thickness of the common piston is less than 10 mm, so $t_0 < 10$ mm. The values of the parameters are shown in Table 2.

Table 2 Values of process parameters

Parameters	1	2	3	4
ξ	0.06	0.14	0.22	0.30
η	0.02	0.10	0.20	0.30
t_0 (mm)	2	4	6	8

SPSS software and the data in Table 2 were used to produce the $L_{16}(4^3)$ orthogonal test table shown in Table 3.

Table 3 $L_{16}(4^3)$ orthogonal experiment table

Series	ξ	η	t_0 (mm)
1	0.06	0.02	8

6

2	0.06	0.1	2
3	0.06	0.2	6
4	0.06	0.3	4
5	0.14	0.02	2
6	0.14	0.1	6
7	0.14	0.2	4
8	0.14	0.3	8
9	0.22	0.02	6
10	0.22	0.1	4
11	0.22	0.2	8
12	0.22	0.3	2
13	0.3	0.02	4
14	0.3	0.1	8
15	0.3	0.2	2
16	0.3	0.3	6

3 Results and discussion

3.1 Typical forming process

Fig. 6 shows a typical material deformation during the DRSP. The material of the blank in the contact area was compressed in the radial and tangential directions and flowed along the two sides of the groove along the axial direc
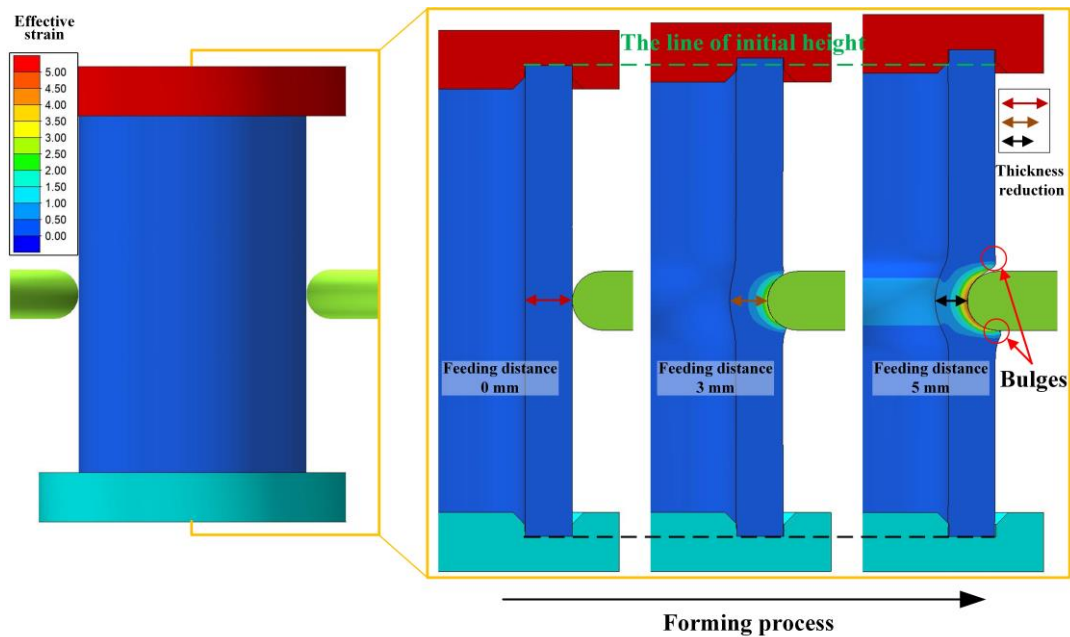
Fig. 6 Typical forming process of DRSP ($\xi = 0.06$, $\eta = 0.02$, $t_0 = 8$ mm)

-tion after the blank was in contact with the rollers. The flow distance in the radial direction of the material close to the inner surface of the blank was smaller than that of the material near the outer surface. A wall-thickness reduction was therefore observed with the rollers feeding in the radial direction. During roller feeding, the deformed material flowing along the axial direction accumulated on the upper and lower sides of the rollers and bulges formed. At the same time, the tube height increased. Throughout the entire forming process, the strains on the upper and lower straight walls of the tube were always zero. The strain in the deformation area increased gradually, and the strain on the outer surface contacting the roller was highest. The strain decreased gradually from the outer to the inner surface

7

and the overall strain increased with roller feeding.

3.2 Comparison of results obtained by simulations and experiments

Fig. 7 shows a comparison of the tubes obtained via simulations and experiments of tests No. 4 and No. 8 in Table 3. The profile of the simulated tube is in good agreement with the longitudinal section obtained by experiments. Fig. 8 shows comparison curves for the thicknesses of the grooves obtained in tests No. 4 and No. 8 via simulations and experiments. Under the two sets of conditions, the thickness distributions obtained by simulations and experiments were similar. The thickness of the grooves was less than t_0, and thickness reduction occurred.

Tube from No.4 test
$\xi = 0.06$, $\eta = 0.3$, $t_0 = 4mm$

Tube from No.8 test
$\xi = 0.14$, $\eta = 0.3$, $t_0 = 8mm$
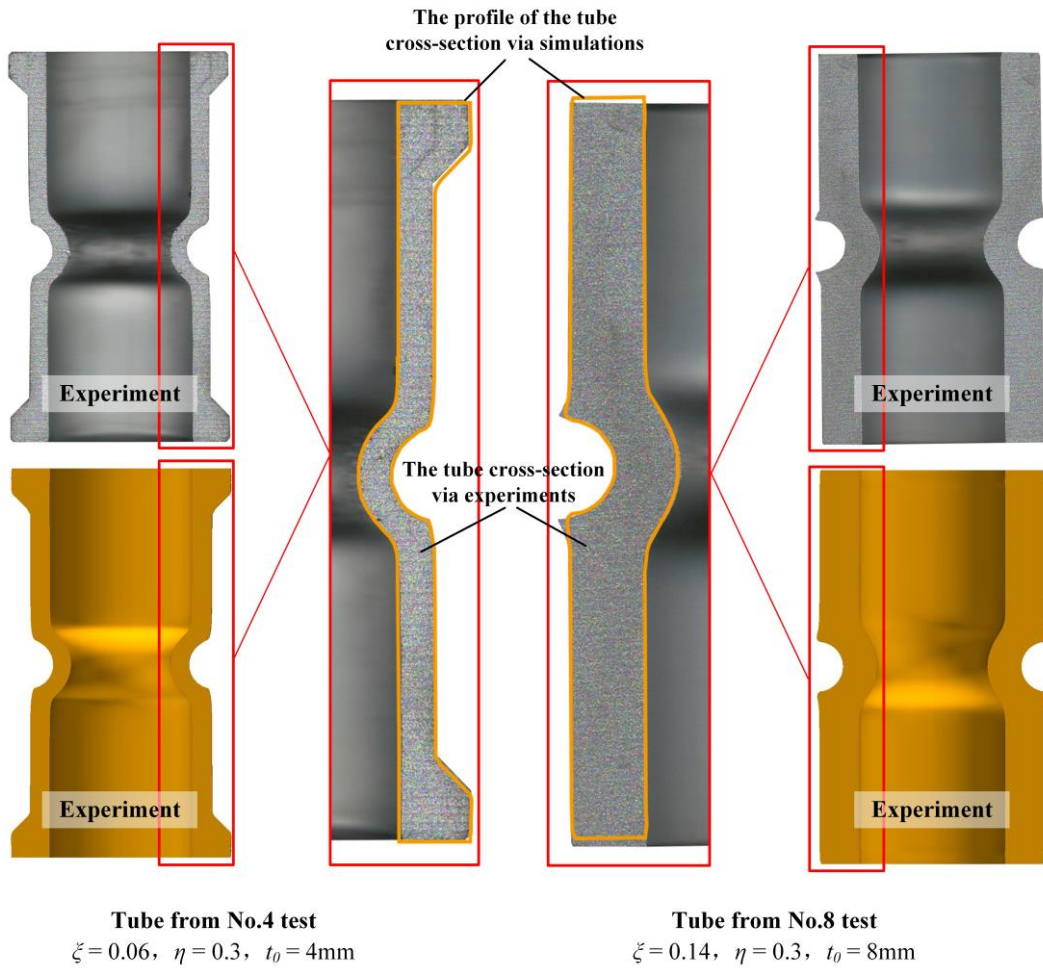
**Fig. 7** Comparison of shapes obtained by experiments and simulations
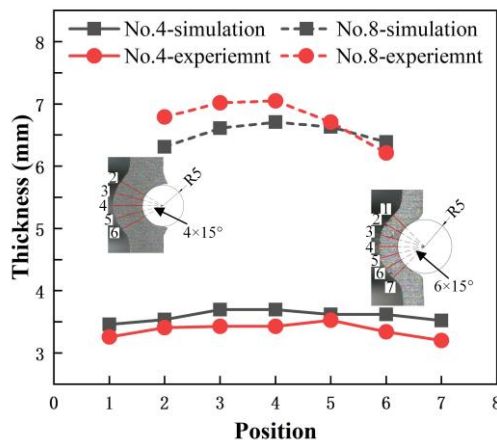
Fig. 8 Comparison curves of groove thicknesses obtained from tests No. 4 and No. 8 by experiments and simulations

3.3 Orthogonal test results

The shape parameters of the blank were taken as the quantitative evaluation indexes in orthogonal tests. The forming quality indicators were the bulge height (the upper bulge height h_u and lower bulge height h_l) on the outer surface, the groove thickness reduction r×ate n, and the tube height h. The bulge height and thickness reduction rate were defined as follows:

$$h_u = (d_u - d_0)/2 \quad (4)$$
$$h_l = (d_l - d_0)/2 \quad (5)$$
$$n = (1 - t/t_0) \times 100\% \quad (6)$$

where d_0 and t_0 are the initial outer diameter and wall thickness, respectively, of the blank; h is the tube height; D_u and D_l are the outer diameter of the upper and lower bulges, respectively; and t is the wall thickness at the groove center. The parameters are shown in Fig. 9. A spinning part with good forming quality requires small absolute values of h_u, h_l, and n.
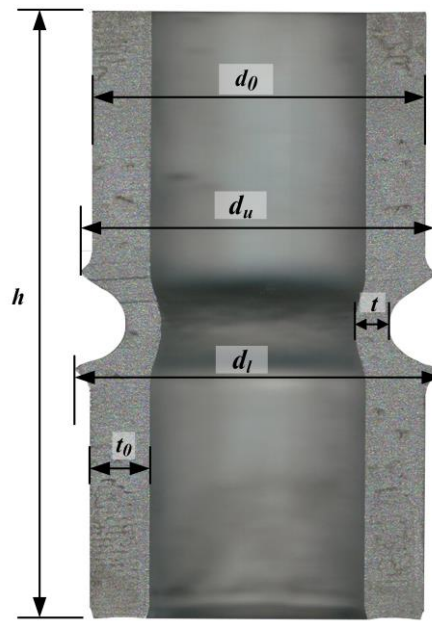

Fig. 9 Schematic diagram of shape parameters

The orthogonal experimental results are shown in Table 4. The data were analyzed by using SPSS, range analysis, and analysis of variance (ANOVA).

Table 4 Experimental orthogonal test data

Series	h(mm)	h_u(mm)	h_l (mm)	t(mm)	n
1	84.2	1.5	2.2	5	37.5%
2	82.3	-0.5	-0.4	/*	/
3	81.45	0.6	0.6	5.2	13.3%
4	81.15	-0.2	-0.2	3.7	7.5%
5	/	/	/	/	/
6	81.2	0.9	1.1	4.8	20%
7	81.25	-0.1	0	3.7	7.5%
8	80.75	1.1	1.1	7.3	8.8%
9	82.2	1.5	2	4.1	31.7%
10	80.7	0.4	0.4	3.5	12.5%
11	81.25	1.1	1.1	7.1	11.3%

12	79.95	-0.7	-0.7	2.1	-5%
13	80.5	1.5	1.5	3.4	15%
14	81.4	1.3	1.5	6.4	20%
15	79.75	-0.6	-0.6	2.1	-5%
16	80.85	0.45	0.5	5.6	6.7%

*The symbol "/" indicates that the data cannot be obtained because of fracture or breakage at the groove.

The results of range analysis of the experimental data in Table 4 are shown in Table 5. More details of the range analysis are given in Appendix A.1. The trends in the effects of the process parameters ξ, η, and t_0 on the measurement indexes h, h_u, h_l, and n are shown in Fig. 10.

Table 5 and Fig. 10 show that the order of the effects of the parameters on h is $\xi > \eta > t_0$. The value of h decreased with increasing ξ and η, and with decreasing t_0. The h value increased slightly relative to that of the initial blank rather than decreasing under most conditions.

The order of the effects of the parameters on h_u and h_l is $t_0 > \eta > \xi$. With increasing ξ, h_u and h_l fluctuated within a small range. Increases in η and decreases in t_0 caused decreases in h_u and h_l.

The order of the effects of the parameters on n was $t_0 > \eta > \xi$. The value of n decreased with increasing ξ and η, and decreased with decreasing t_0.

Table 5 Range analysis results

| Parameters	Indexes	k_1	k_2	k_3	k_4	R
ξ	h	82.28	81.07	81.03	80.63	1.65
	h_u	0.35	0.63	0.58	0.66	0.31
	h_l	0.55	0.73	0.7	0.73	0.18
	n	19.4	12.1	12.6	9.2	10.2
η	h	82.3	81.4	80.93	80.68	1.62
	h_u	1.5	0.53	0.25	0.16	1.34
	h_l	1.9	0.65	0.28	0.18	1.72
	n	28.1	17.5	6.8	4.5	23.6
t_0	h	80.67	80.90	81.43	81.90	1.23
	h_u	-0.6	0.4	0.86	1.25	1.85
	h_l	-0.57	0.43	1.05	1.48	2.05
	n	-5	10.6	17.9	19.4	24.4
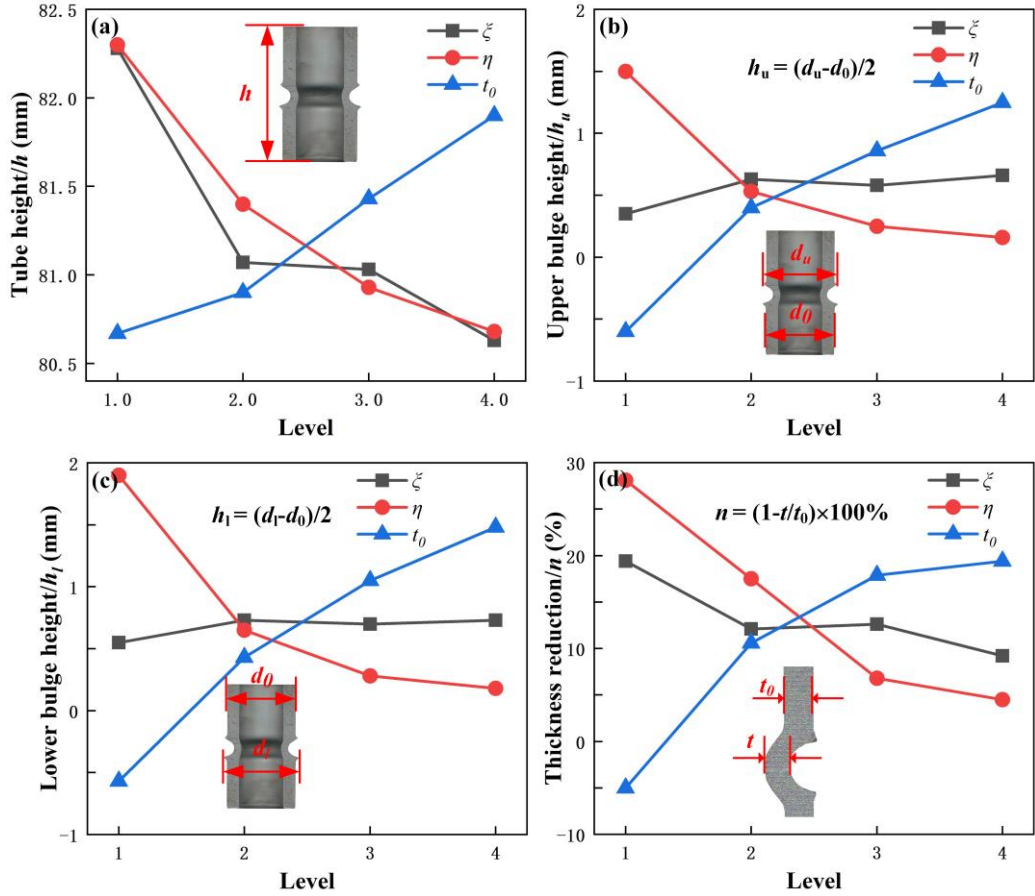
Fig. 10 Effects of process parameters on measurement indexes according to range analysis

The analysis of variance (ANOVA) results for the experimental data in Table 3 are shown in Table 6. More details of the ANOVA process are given in Appendix A.2.

Table 6 Analysis of variance

Indexes	Parameters	S	f	M	F	Significance*
h	ξ	3.107	3	1.036	1.833	No significance
	η	3.132	3	1.044	1.848	No significance
	t_0	2.647	3	0.882	1.562	No significance
	Error	2.260	4	0.565		
h_u	ξ	0.197	3	0.066	0.791	No significance
	η	1.734	3	0.578	6.953	Significance
	t_0	3.4	3	1.133	13.632	Significance
	Error	0.333	4	0.083		
h_l	ξ	0.059	3	0.020	1.81	No significance
	η	3.476	3	1.159	107.459	Significance
	t_0	3.984	3	1.328	123.169	Significance
	Error	0.043	4	0.011		
n	ξ	0.011	3	0.004	2.730	No significance
	η	0.073	3	0.024	18.924	Significance
	t_0	0.032	3	0.011	8.33	Significance
	Error	0.005	4	0.001		

*$F_{0.05}(3, 4) = 6.59$ (critical value obtained by looking up F distribution table).

11

The data in Table 6 show that ξ, η, and t_0 had no significant effects on h. The values of h_u, h_l, and n were significantly affected by t_0 and η, but ξ had no significant effects.

Fig. 10(a) shows that each process parameter had a certain influence on h, but the ANOVA results show that the effects were not significant.

3.4 Effects of process parameters on forming quality

According to the results via experiments and simulations, two phenomena—bulge formation and thickness reduction—affect the forming quality of the spinning parts. The h_u, h_l, n, and h values are important indexes in evaluation of the forming quality. The effects of the process parameters on the indexes were therefore investigated.

3.4.1 Thickness reduction at groove

Feeding in the radial direction of the rollers leads to bending of the wall of the deformation area and groove formed. The change in the material volume in the forming area after forming was calculated, with the assumption that the wall thickness at the groove remained constant, as shown in Fig. 11.
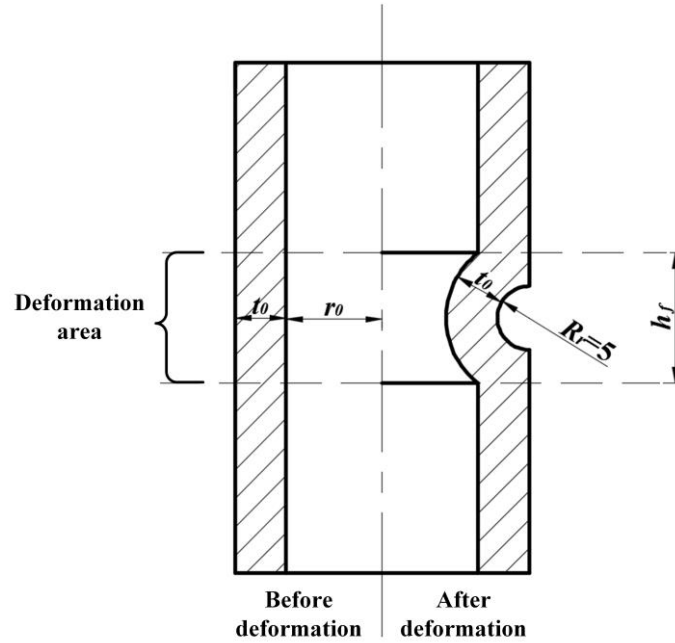
Fig. 11 Change in deformation area before and after spinning, with assumption that wall thickness remains constant

In Fig. 11, R_r is the radius of the groove and h_f is the height of the deformation area.

$$h_f = 2\sqrt{(R_r+t_0)^2 - t_0^2} = \sqrt{10t_0 + 25} \quad (7)$$

A combination of Eq. (7) and a geometric formula gives the volume of the forming area before spinning:

$$V_{before} = h_f \cdot \pi[(r_0+t_0)^2 - r_0^2] = 2\pi(30t_0 + t_0^2)\sqrt{10t_0 + 25} \quad (8)$$

The volume of the forming area after spinning is

$$V_{after} = 2\pi\left\{\int_0^{R_r}\left[\left(r_0+t_0-\sqrt{R_r-x^2}\right)^2 - \left(r_0+t_0-\sqrt{(R_r+t_0)^2-x^2}\right)^2\right]dx + \int_{R_r}^{\frac{h_f}{2}}\left[(r_0+t_0)^2 - \left(r_0+t_0-\sqrt{(R_r+t_0)^2-x^2}\right)^2\right]dx\right\} \quad (9)$$

$$\Delta V = \frac{V_{after} - V_{before}}{V_{before}} \times 100\% \quad (10)$$

Eq. (7-10) were used to calculate the theoretical changes in the volume of the deformation area for different t_0 values; the results are shown in Table 7. If the wall thickness of the deformation area is unchanged during the deformation, the volume increases. However, the volume should be invariant, therefore the wall thickness should

12

decrease.

The experimental results show that there was thickening at the groove under certain sets of parameters (tests No.12 and No.15 in Table 4). According to Fig. 10(b) and (c), when t_0 was small and η was large simultaneously, bulge formation was prevented and even concavity formed. However, the thickness reduction rate declined. This means more material flowed to the middle of the groove, which can lead to thickening.

Table 7 Volumes of deformation area before and after spinning, with assumption that wall thickness remains constant, for different t_0 values

t_0/mm	V_{before}/mm³	V_{after}/mm³	ΔV
2	3032.3	3368.4	12.50%
4	7411.9	7938	7.60%
6	12506.1	13133.9	5.00%
8	19562.7	20231.5	3.40%

Fig. 12 shows the strain distributions during the forming process in the deformation area for the same t_0 and ξ, but different η. The figure shows that the strain on the outer surface of the deformation area was significantly larger, the wall at the groove was thinner, and n was larger for the tube with $\eta = 0.02$ than in the case with $\eta = 0.3$. This is consistent with the finding that n decreased with increasing η, as shown in Fig. 10(d).
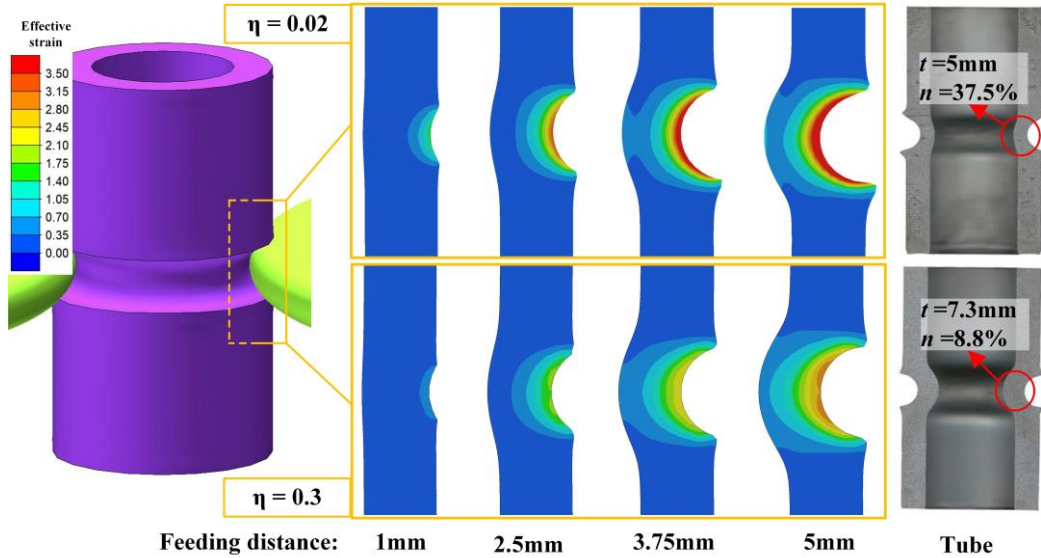
Fig. 12 Strain distributions in deformation area at different feeding distances ($t_0 = 8$ mm, $\xi = 0.14$, $\eta = 0.02$ and 0.30)

Fig. 13 shows the strain distributions at the middle of the groove from outside to inside for different η values when $\xi = 0.14$ and $t_0 = 8$ mm. The figure shows that from the outer surface to the inner surface, the strain value first decreased and then stabilized. The strain near the outer surface of the groove increased with decreasing η, but the strain near the inner surface did not noticeably change.
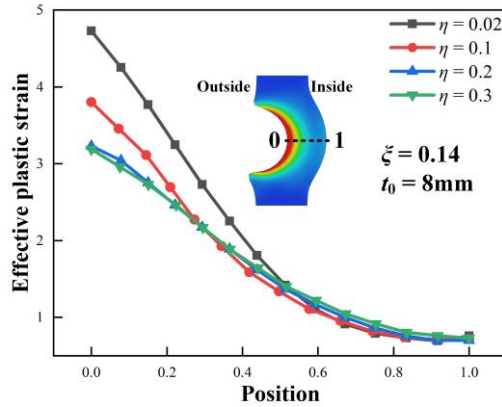
Fig. 13 Strain distributions at middle of groove at different η values ($\xi = 0.14$, $t_0 = 8$ mm)

The outer surface of the blank suffered from friction and rolling of the rollers, therefore the strain there was large. There was no direct contact between the inner surface and the rollers, therefore the strain decreased from outside to inside. The forming time was longer for a smaller η, and the time of interaction between the rollers and the blank outer surface was longer, which led to increased strain. The strain changed little with changes in η because the impact of the rollers' action was small near the inner surface.

A larger difference between the strain values at the inner and outer surfaces in the groove means more uneven deformation of the internal and external material, and shows that more material flowed to the area outside the groove, that is, a smaller wall thickness of the groove and larger n. A smaller η therefore gives a larger n. Fig. 14 shows that the grooves of the tubes obtained by experiments in tests No. 2 and No. 5 were cracked or even broken. This is because the smaller η led to a larger n, and the initial wall thickness in both cases was small.
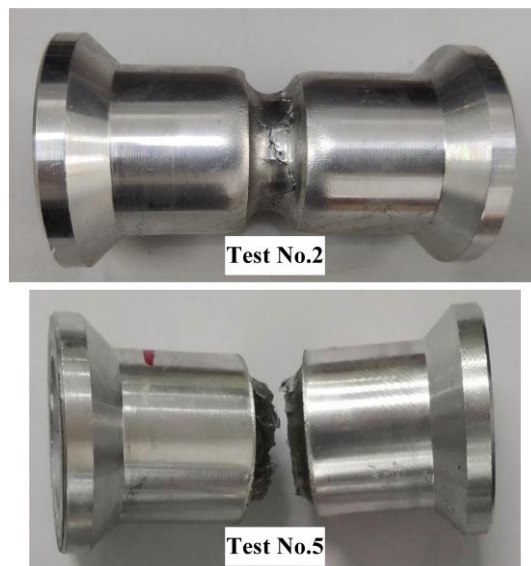
Fig. 14 Tubes obtained by experiments in tests No. 2 and No. 5

Fig. 15 shows tubes with $\eta = 0.02$ and $t_0 = 4$, 8 mm; the n of the tube with $t_0 = 4$ mm was 15%, and that with $t_0 = 8$ mm was 37.5%.
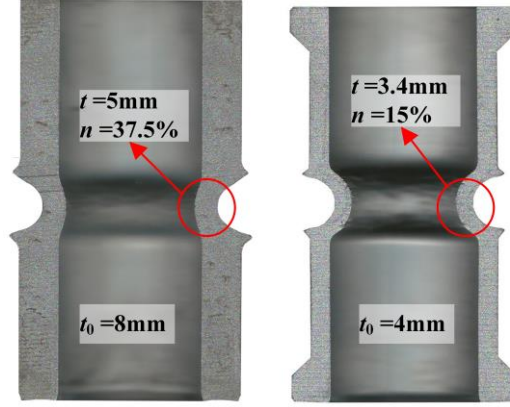
Fig. 15 Axial profiles of tubes obtained by experiments with $\eta = 0.02$ and $t_0 = 4, 8$ mm

Fig. 16 shows an axial profile schematic diagram of the DRSP. It is assumed that the thickness of the groove was uniform; r_0 is the inner diameter of the blank, R_r is the rim radius of the roller, and t is the wall thickness of the groove.
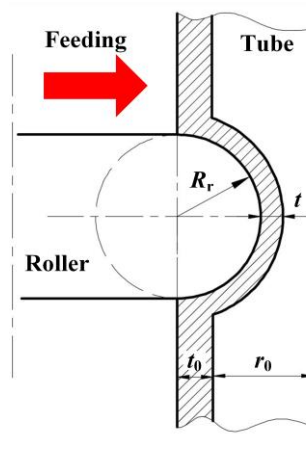

Fig. 16 Axial profile schematic diagram of DRSP, with assumption that groove thickness was uniform

The average axial strain of the groove can be calculated from the arc length l and the initial length l_0 because the change in h was small and can be ignored, according to the experimental results:

$$\varepsilon_z = ln\left(\frac{l}{l_0}\right) = ln\left(\frac{\pi R_r}{2R_r}\right) = ln\left(\frac{\pi}{2}\right) \quad (11)$$

The circumferential strain can be calculated as the natural logarithm of the circumference ratio:

$$\varepsilon_\theta = ln\left(\frac{2(r_0+t_0-R_r)\pi}{2(r_0+t_0)\pi}\right) = ln\left(\frac{r_0+t_0-R_r}{r_0+t_0}\right) \quad (12)$$

According to the principle of volume invariance, the radial strain can be expressed as

$$\varepsilon_r = -(\varepsilon_z+\varepsilon_\theta) = ln\left(\frac{2}{\pi}\left(1+\frac{R_r}{r_0+t_0-R_r}\right)\right) \quad (13)$$

The radial strain is the natural logarithm of the wall thickness ratio. From Eq. (13), the ratio of the wall thickness of the groove to the initial wall thickness can be expressed as

$$\frac{t}{t_0} = \frac{2}{\pi}\left(1+\frac{R_r}{r_0+t_0-R_r}\right) \quad (14)$$

The ratio of the wall thickness of the groove to the initial wall thickness decreased with increasing t_0, i.e., n increased.

Fig. 17 and Fig. 18 show the strain distributions of grooves with different t_0 values when $\xi = 0.14$ and $\eta = 0.2$.

15

The figures show that the strain on the outer surface of the groove increased and the strain on the inner surface decreased with increasing t_0; that is , the deformation near the outer surface increased and that near the inner surface decreased. Fig. 19 shows deformations of grooves with different t_0 values and the same feeding distance. The deformation of the inner wall was smaller when t_0 was larger, and the radial resistance of the material was greater during roller feeding. More material flowed up and down, and n increased.
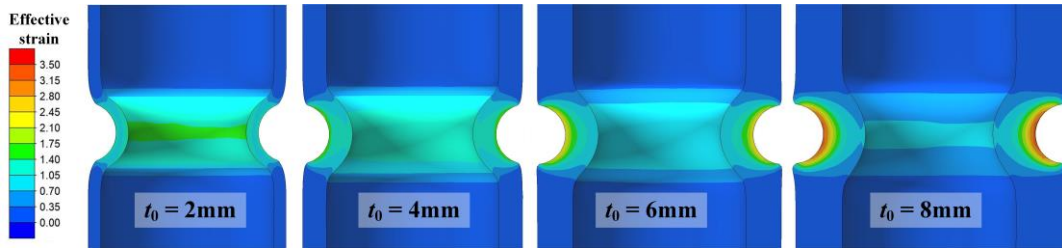
Fig. 17 Strain distribution of the tubes with different t_0 via simulations($\xi = 0.14$, $\eta = 0.2$)
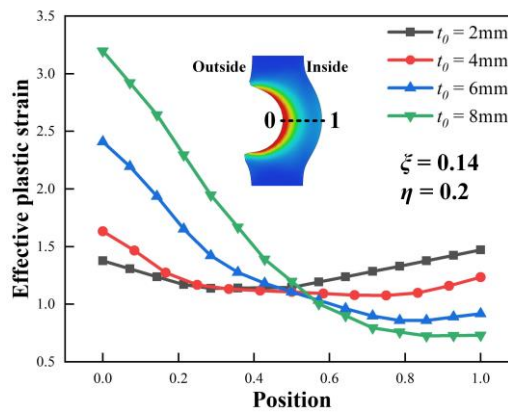
Fig. 18 Strain distribution curves of grooves with different t_0 via simulations ($\xi = 0.14$, $\eta = 0.2$)
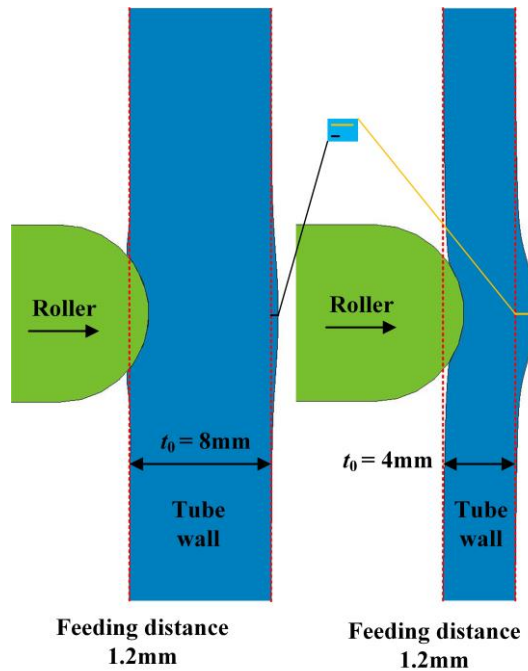
Fig. 19 Deformations of grooves with different t_0 values and feeding distance 1.2 mm ($\xi = 0.14$, $\eta = 0.2$, $t_0 = 8$, 4 mm)

Fig. 20 shows the strain distributions of grooves with different ξ values when $\eta = 0.2$ and $t_0 = 6$ mm. The figure shows that the strain distributions of the grooves near the inner surface changed little with changes in ξ, but the strains
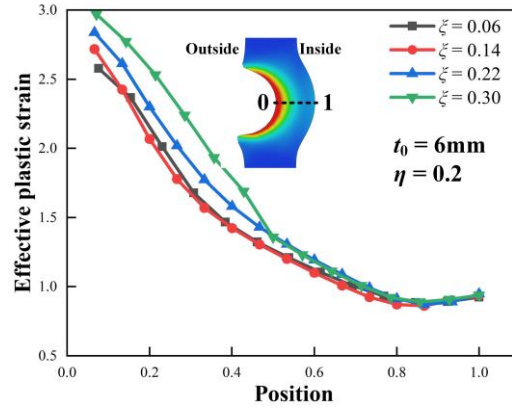
Fig. 20 Strain distributions of grooves with different ξ values ($\eta = 0.2$, $t_0 = 6$ mm)

close to the outer surface increased with increasing ξ. The maximum strain difference at the same position of the grooves with different ξ values was smaller than 0.5. It can be concluded that ξ had little effect on the material flow during the forming process, therefore the effect of ξ on the n values of the grooves was not significant.

3.4.2 Bulges

According to the analysis in section 4.4.1, the wall thickness of the groove decreased during radial spinning. This thickness reduction means that some material flowed from the groove to both sides, and bulges formed.

Fig. 21 shows the bulges formed on both sides of the groove in experiments with different η values; a small η promoted the emergence of bulges. Fig. 22 shows the radial stress distributions of the deformation zone at η values of 0.02 and 0.30, with a feeding distance of 3 mm. The areas on both sides of the roller were under tensile stress in the radial direction when η was small, but the stress became compressive at high η values. Compressive stress can prevent bulge formation. The h_u and h_l values therefore decreased with increasing η.
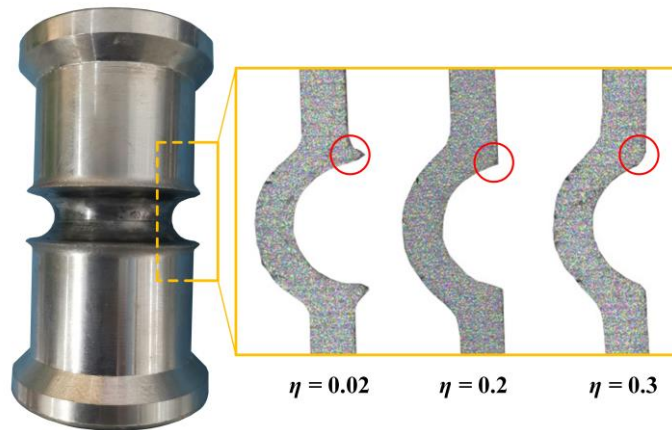

Fig. 21 Upper/lower bulges formed in tubes during experiments with different η values ($t_0 = 4$ mm, $\xi = 0.14$)

17
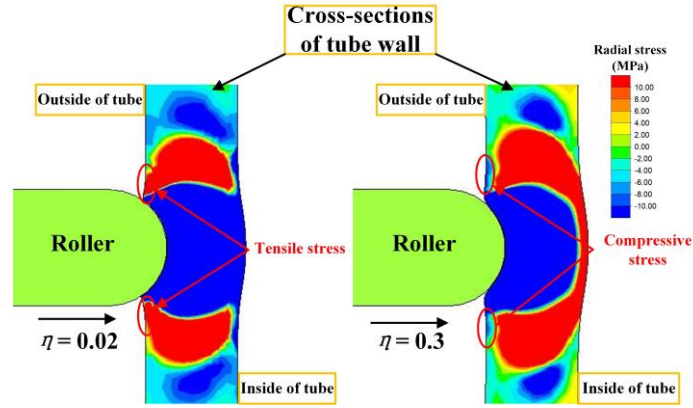
Fig. 22 Radial stress distributions of deformation zones at different η values and feeding distance of 3 mm ($t_0 = 8$ mm, $\xi = 0.14$)

Fig. 23 shows longitudinal sections of tubes via experiments with different t_0 values. The figure shows that h_u and h_l increased with increasing t_0. The flexural capacity was weak when the tube wall was thin. The radial force from the rollers made the wall bend. That counteracted some plastic deformation. Fewer materials flowed upside and downside, and the height of bulges was smaller. When the bulge could not compensate the bending, concavity appeared. Conversely, the flexural capacity was strong for the thick tube wall. More plastic deformation occurred pushed by the roller, that is, more materials flowed to the both sides, and higher bulges formed. That is shown in Fig. 19.
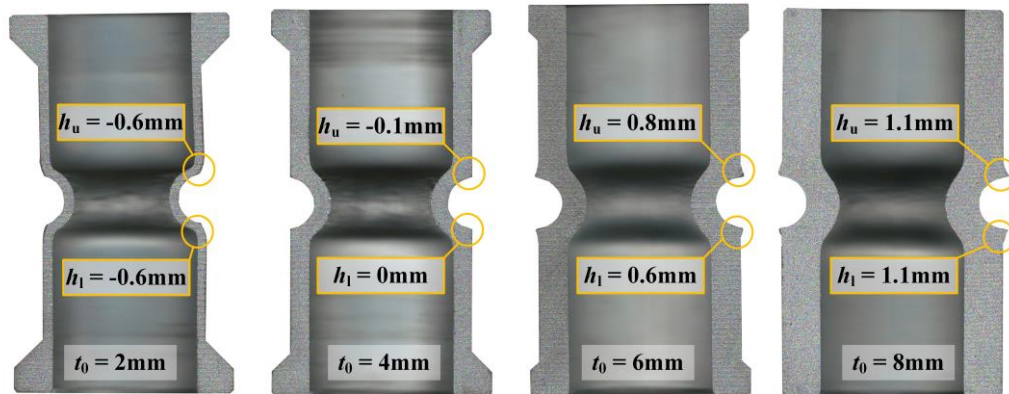
Fig. 23 Upper/lower bulges formed in tubes during experiments with different t_0 values ($\eta = 0.2$, $\xi = 0.14$)

As shown in section 4.4.1, ξ had little effect on the material flow of the blank during the forming process and therefore had little effect on h_u and h_l.

3.4.3 Tube height

The ANOVA results show that the three factors had no significant effect on h. However, the range analysis results show that there were influence rules of each parameter on h.

During roller feeding, the roller produced an axial force on the upper and lower straight walls. The lower die was fixed, and the upper die was controlled by ξ. The upper straight wall could be lifted when ξ was small, which would increase h.

The pressure of the upper die increased with increasing ξ, more material flowed to the groove or bulge, and the increase in h was suppressed. However, the amount of material involved in deformation was small relative to that in the whole tube. The material flow caused by the pressure of the upper die, that is, ξ, therefore made little difference to h.

As discussed in sections 4.4.1 and 4.4.2, h_u, h_l, and n decreased with increasing η and with decreasing t_0; this suppressed the increase in h. Similarly, the effect was small because the change in the amount of material involved

in deformation was small relative to that in the whole tube.

3.5 Definition of processing window

As discussed in section 4.4, thickness reduction and bulge formation are major indexes for evaluating the forming quality. These were significantly affected by t_0 and η. According to the general accuracy requirement for thick-walled cylindrical parts with annular grooves, if h_b (the average of h_u and h_l) and n, respectively, meet the criteria -0.5 mm $\leq h_b \leq 0.5$ mm and $-10\% \leq n \leq 10\%$, the tube is considered to be an eligible part.

Fig. 24 shows the forming qualities at different t_0 and η values through the experimental results of orthogonal tests. Only three parts (with $t_0 = 4$ mm and $\eta = 0.2$, $t_0 = 4$ mm and $\eta = 0.3$, and $t_0 = 6$ mm and $\eta = 0.3$) were completely eligible. When t_0 and η were too small or too large, the grooves had defects; that is, they were over-swollen, over-sunken, over-thin, cracked, or broken. The results suggest that t_0 should be set at 4–6 mm; the selected η value should be 0.2 when $t_0 = 4$ mm, and 0.2–0.3 when $t_0 = 6$ mm.
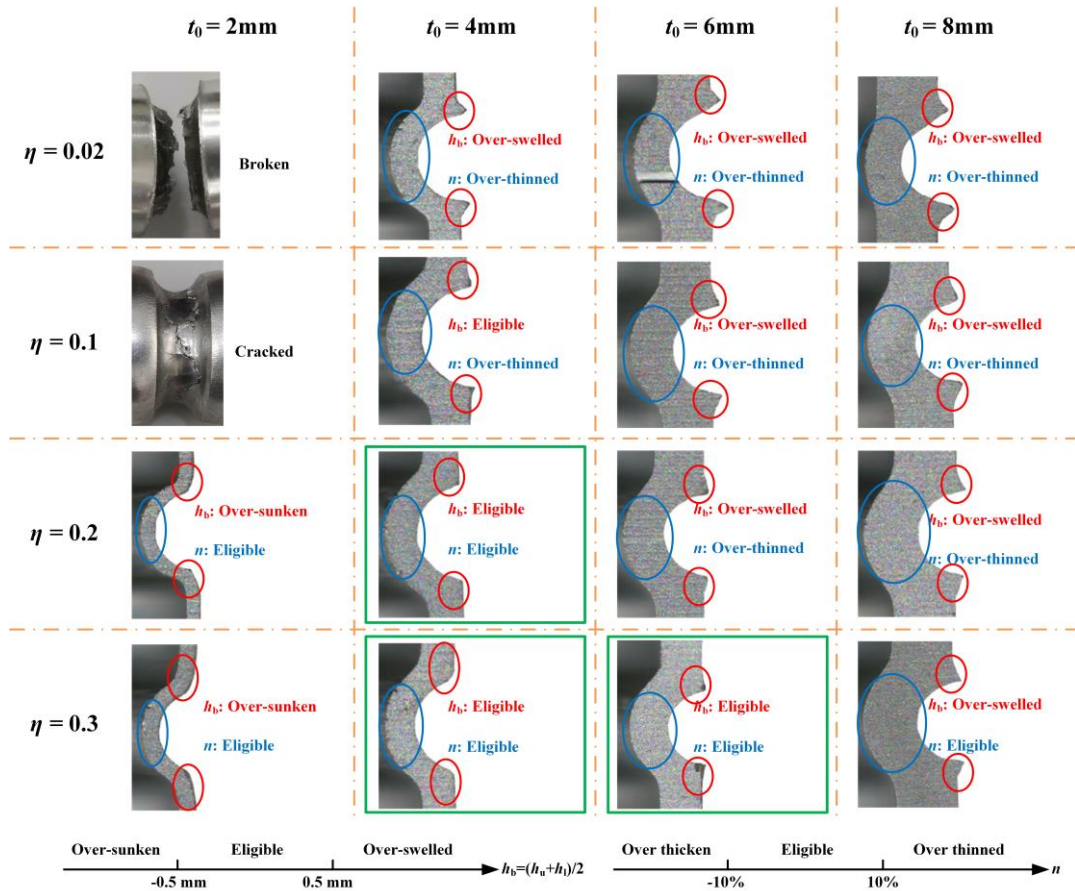
Fig. 24 The forming qualities with different t_0 and η values obtained by experiments

4 Conclusions

In this study, orthogonal experiments and simulations were performed to investigate the DRSP with double rollers. The experimental and simulation results were in good agreement. The effects and mechanisms of the process parameters on the forming quality were analyzed. The following conclusions were drawn.

(1) In the forming process, the material in contact with the rollers shrinks in the radial and tangential directions of the blank because of roller feeding. Meanwhile, some material flows along the axial direction to both sides of the groove. This can decrease the groove thickness and cause formation of upper and lower bulges.

(2) Range analysis and ANOVA results show that the stress yield ratio has no significant effect on the forming quality of the tube. The feed thickness ratio and initial wall thickness have significant effects on the thickness

reduction ratio and bulge heights. In the case of bulge height, the effect of the initial wall thickness is greater than that of the feed thickness ratio. For the thickness reduction ratio, the two effects are approximately equal. None of the investigated parameters significantly affected the tube height.

(3) The thickness reduction ratio, bulge heights, and tube heights decrease with increasing feed thickness ratio. All three indexes increase with increasing initial thickness of the blank.

(4) The difference of deformation between the thick and thin wall was caused by the difference flexural capacity. Only when the plastic deformation and bending counteracted with each other, bulges and concavity would not appear.

(5) The experimental results show that to ensure good forming quality, the initial wall thickness of the blank should be set at 4–6 mm, and the selected feed thickness ratio should be 0.2 when $t_0 = 4$ mm and 0.2–0.3 when $t_0 = 6$ mm.

Ethical Approval

Not applicable.

Consent to Participate

Not applicable.

Consent to Publish

Not applicable.

Authors Contributions

Famei Liu: experiment, data analysis, simulated analysis, original draft writing
Junsong Jin: methodology, experiment, review and editing
Wei Rao: experiment, formal analysis, original draft writing
Ying Wang: experiment
Chang Gao: experiment
Xuefeng Tang: experiment
Xinyun Wang: review and editing

Funding

Competing Interests

The authors declare no competing interests

Availability of data and materials

All data generated or analyzed during this study are included in this manuscript.

Acknowledgments

Appendix A

A.1 Range analysis

Range analysis was used to compare the effects of various factors on target indexes by calculating the range.

In Table 4, k_i refers to the average value of the index at No. i level and R represents the maximum difference among the k_i values, i.e., $R = \max(k_i) - \min(k_i)$. The change in k_i indicates the trend in the effect of the factor. As the value of R increases, the effect of the factor on the index becomes more significant [21].

A.2 Analysis of variance

Variance analysis was used to evaluate the effects of factors on target parameters.

In Table 5, S refers to the sum of the squared deviations (DEVSQ) of the factor; f is the degree of freedom (DOF); M is the average DEVSQ, namely the ratio of DEVSQ to DOF; F is the standard for evaluating the significance and equals M of the factor divided by M of the error. Given a significance level β, the critical value $F_\beta(f_i, f_e)$ can be obtained by consulting the critical value table of the F distribution. The significance can be evaluated by comparing F and $F_\beta(f_i, f_e)$, where F_i and F_e are the DOF of the factor and error, respectively [21].

In this study, the DOF of the process parameters was 3 and the DOF of the error was 4. The critical value $F_{0.05}(3, 4) = 6.59$ was obtained from the critical value table of F distributions. When $F < F_{0.05}(3, 4)$, it is considered that the effect of the process parameters on the indexes is not significant; when $F > F_{0.05}(3, 4)$, it is considered that the effect of the process parameters on the indexes is significant.

Reference

[1] Zhan M, Yang H, Guo J, Wang X (2015) Review on hot spinning for difficult-to-deform lightweight metals. T Nonferr Metal Soc 25:1732-1743. https://doi.org/10.1016/S1003-6326(15)63778-5

[2] Yuan S, Xia Q, Long J, Xiao G, Cheng X (2020) Study of the microstructures and mechanical properties of ZK61 magnesium alloy cylindrical parts with inner ribs formed by hot power spinning. Int J Adv Manuf Tech 111:851-860. https://doi.org/10.1007/s00170-020-06091-2

[3] Music O, Allwood JM, Kawai K (2010) A review of the mechanics of metal spinning. J Mater Process Tech 210:3-23. https://doi.org/10.1016/j.jmatprotec.2009.08.021

[4] Wong CC, Dean TA, Lin J (2003) A review of spinning, shear forming and flow forming processes. Int J Mach Tool Manu 43:1419-1435. https://doi.org/10.1016/j.jmatprotec.2009.08.02110.1016/S0890-6955(03)00172-X

[5] Parsa MH, Pazooki AMA, Nili Ahmadabadi M (2009) Flow-forming and flow formability simulation. Int J Adv Manuf Tech 42:463-473. https://doi.org/10.1007/s00170-008-1624-0

[6] Huang C, Hung J, Hung C, Lin C (2011) Finite element analysis on neck-spinning process of tube at elevated temperature. Int J Adv Manuf Tech 56:1039-1048. https://doi.org/10.1007/s00170-011-3247-0

[7] Zoghi H, Fallahi Arezoodar A, Sayeaftabi M (2013) Enhanced finite element analysis of material deformation and strain distribution in spinning of 42CrMo steel tubes at elevated temperature. Mater Design 47:234-242. https://doi.org/10.1016/j.matdes.2012.11.049

[8] Xia QX, Xie SW, Huo YL, Ruan F (2008) Numerical simulation and experimental research on the multi-pass neck-spinning of non-axisymmetric offset tube. J Mater Process Tech 206:500-508. https://doi.org/10.1016/j.jmatprotec.2007.12.066

[9] Xia Q, Cheng X, Long H, Ruan F (2012) Finite element analysis and experimental investigation on deformation mechanism of non-axisymmetric tube spinning. Int J Adv Manuf Tech 59:263-272. https://doi.org/10.1007/s00170-011-3494-0

[10] Arai H (2019) Noncircular tube spinning based on three-dimensional CAD model. Int J Mach Tool Manu 144:103426. https://doi.org/10.1016/j.ijmachtools.2019.103426

[11] Yao J, Makoto M (2002) An experimental study on paraxial spinning of one tube end. J Mater Process Tech 128:324-329. https://doi.org/10.1016/S0924-0136(02)00473-9

[12] Kwiatkowski L, Tekkaya AE, Kleiner M (2013) Fundamentals for controlling thickness and surface quality during dieless necking-in of tubes by spinning. CIRP Annals 62:299-302. https://doi.org/10.1016/j.cirp.2013.03.054

[13] Yao J, Makoto M (2002) Effects of indented feed of roller tool on parallel spinning of circular aluminum tube. J Mater Process Tech 128:274-279. https://doi.org/10.1016/S0924-0136(02)00465-X

[14] Guo X, Li B, Jin K, Wang H, Wan B, Tao J (2017) A simulation and experiment study on paraxial spinning of Ni-based superalloy tube. Int J Adv Manuf Tech 93:4399-4407. https://doi.org/10.1007/s00170-017-0855-3

[15] Grzancic G, Löbbe C, Ben Khalifa N, Tekkaya AE (2019) Analytical prediction of wall thickness reduction and forming forces during the radial indentation process in Incremental Profile Forming. J Mater Process Tech 267:68-79. https://doi.org/10.1016/j.jmatprotec.2018.12.003

[16] Zhu C, Zhao S, Li S, Fan S (2019) Comparison of mandrel and counter-roller spinning methods for manufacturing large sheaves. Int J Adv Manuf Tech 100:409-419. https://doi.org/10.1007/s00170-018-2707-1

[17] Yu Z, Zhao Y, Du C, Liu R, Evsyukov SA (2020) Study on flange-constrained spinning process for hemispherical aluminum alloy part. J Mater Process Tech 278:116515. https://doi.org/10.1016/j.jmatprotec.2019.116515

[18] Li Z, Shu X (2019) Numerical and experimental analysis on multi-pass conventional spinning of the cylindrical part with GH3030. Int J Adv Manuf Tech 103:2893-2901. https://doi.org/10.1007/s00170-019-03767-2

[19] Guo Y, Li M, Xu H, Li L, Wang L, Luo W, Zheng H, et al (2018) Research on multi-pass hot spinning based on finite element simulation and experiment for aluminum alloy component. Int J Adv Manuf Tech 97:1995-2008. https://doi.org/10.1007/s00170-018-2057-z

[20] Zhan M, Guo J, Fu MW, Li R, Gao PF, Long H, Ma F (2018) Formation mechanism and control of flaring in forward tube spinning. Int J Adv Manuf Tech 94:59-72. https://doi.org/10.1007/s00170-017-0690-6

[21] Wang X, Li L, Deng L, Jin J, Hu Y (2015) Effect of forming parameters on sheet metal stability during a rotary forming process for rim thickening. J Mater Process Tech 223:262-273. https://doi.org/10.1016/10.1016/j.jmatprotec.2015.04.009
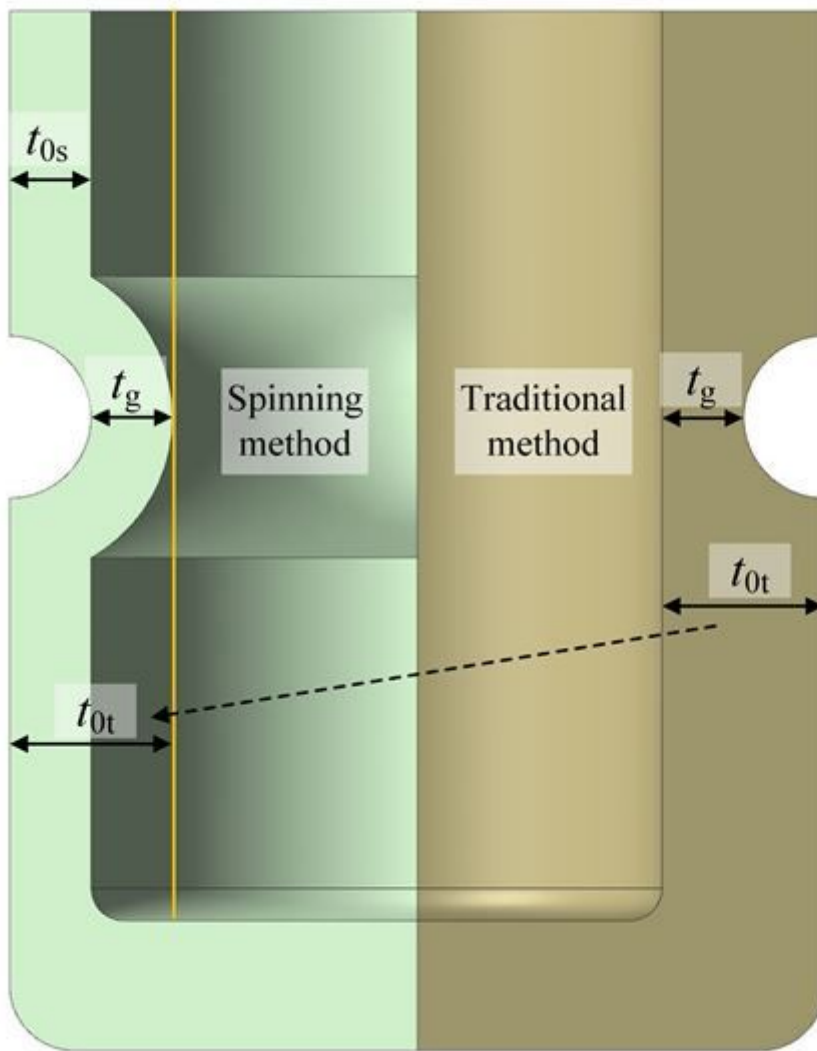
Figures

Figure 1

Comparison of initial thickness between spinning method and traditional method
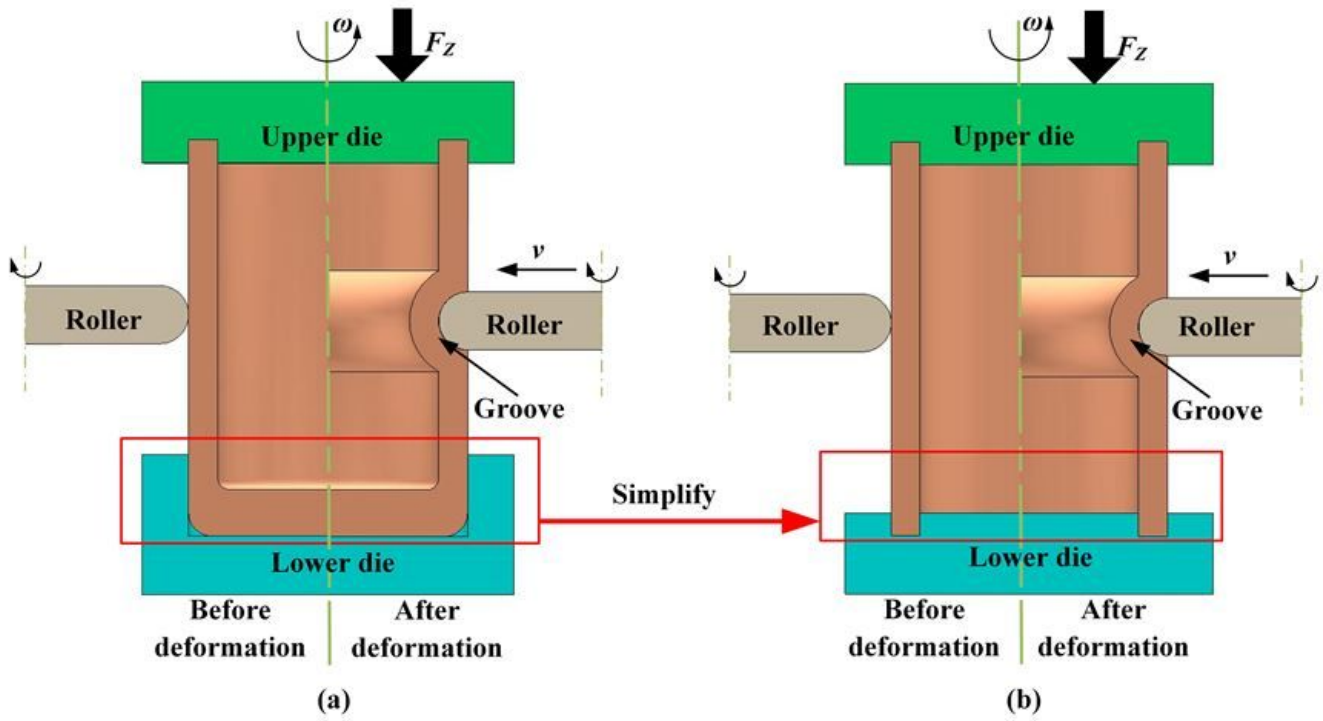
Figure 2

Schematic diagram of DRSP: (a) original model and (b) simplified model
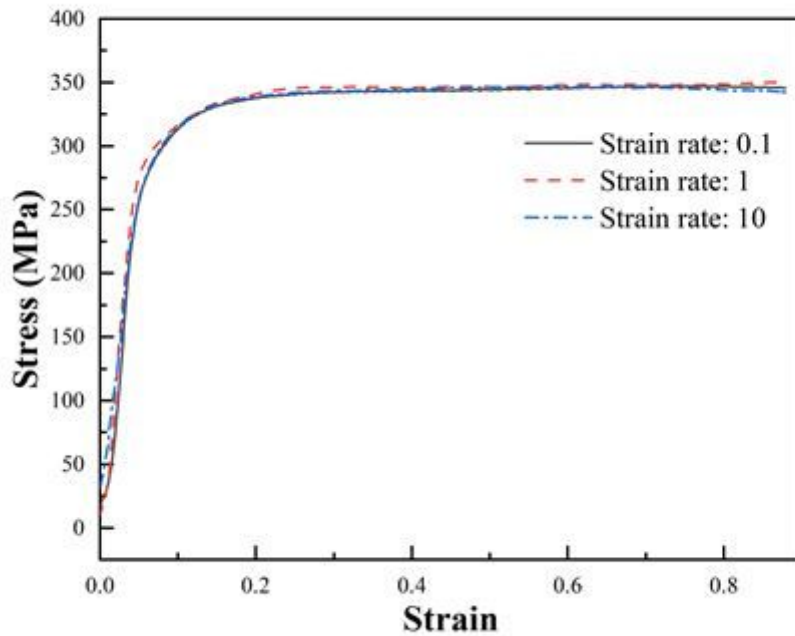
Figure 3

True stress−strain curve of 6061 aluminum alloy
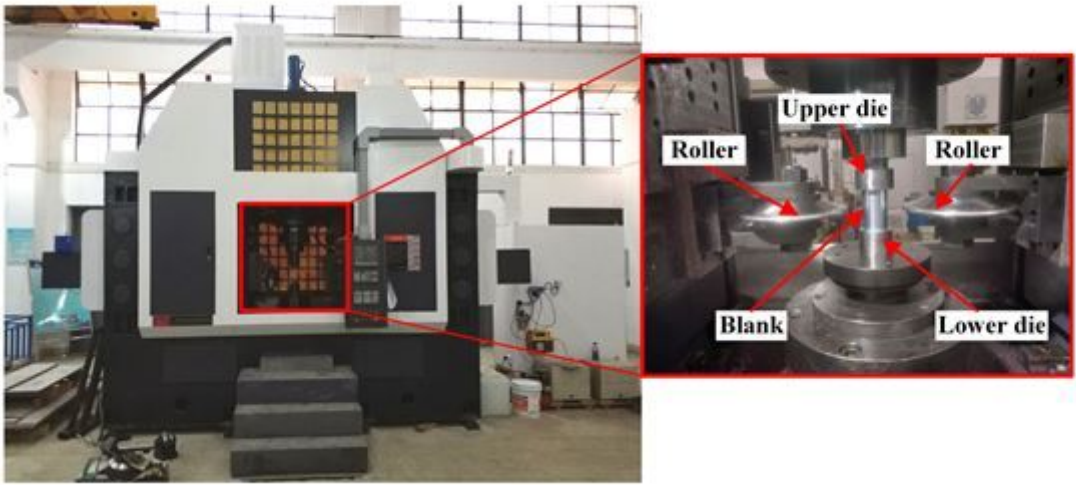
Figure 4

PS-CNCVGP450 vertical CNC spinning machine and molds
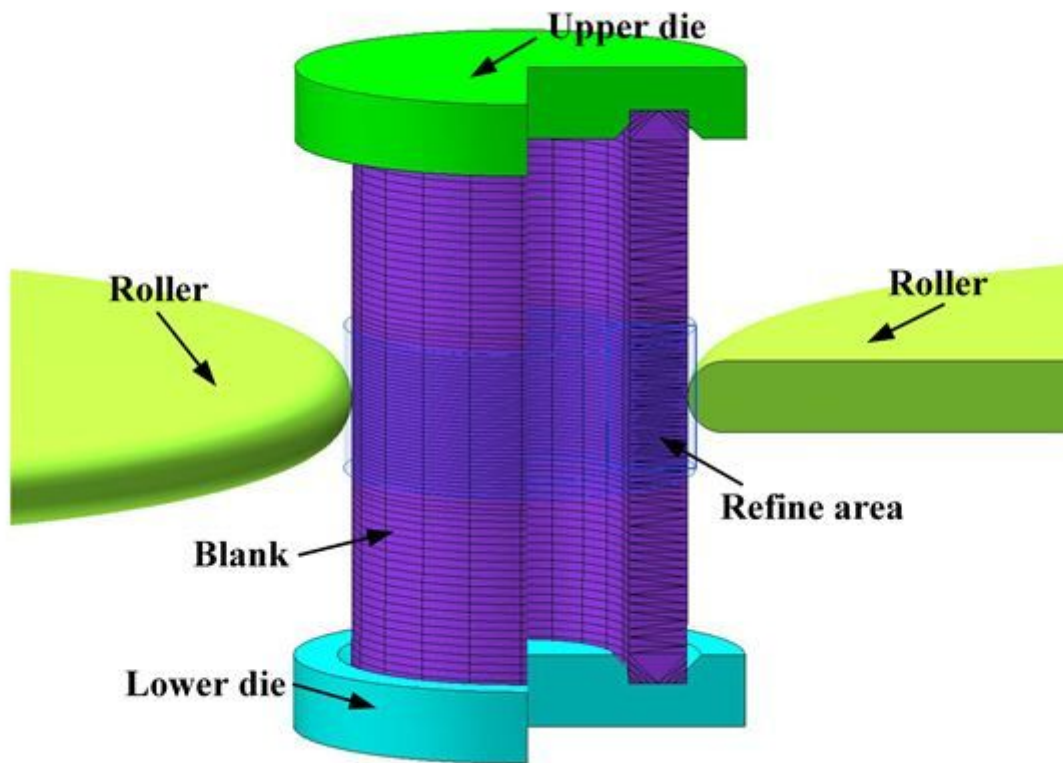
Figure 5

FE model of DRSP
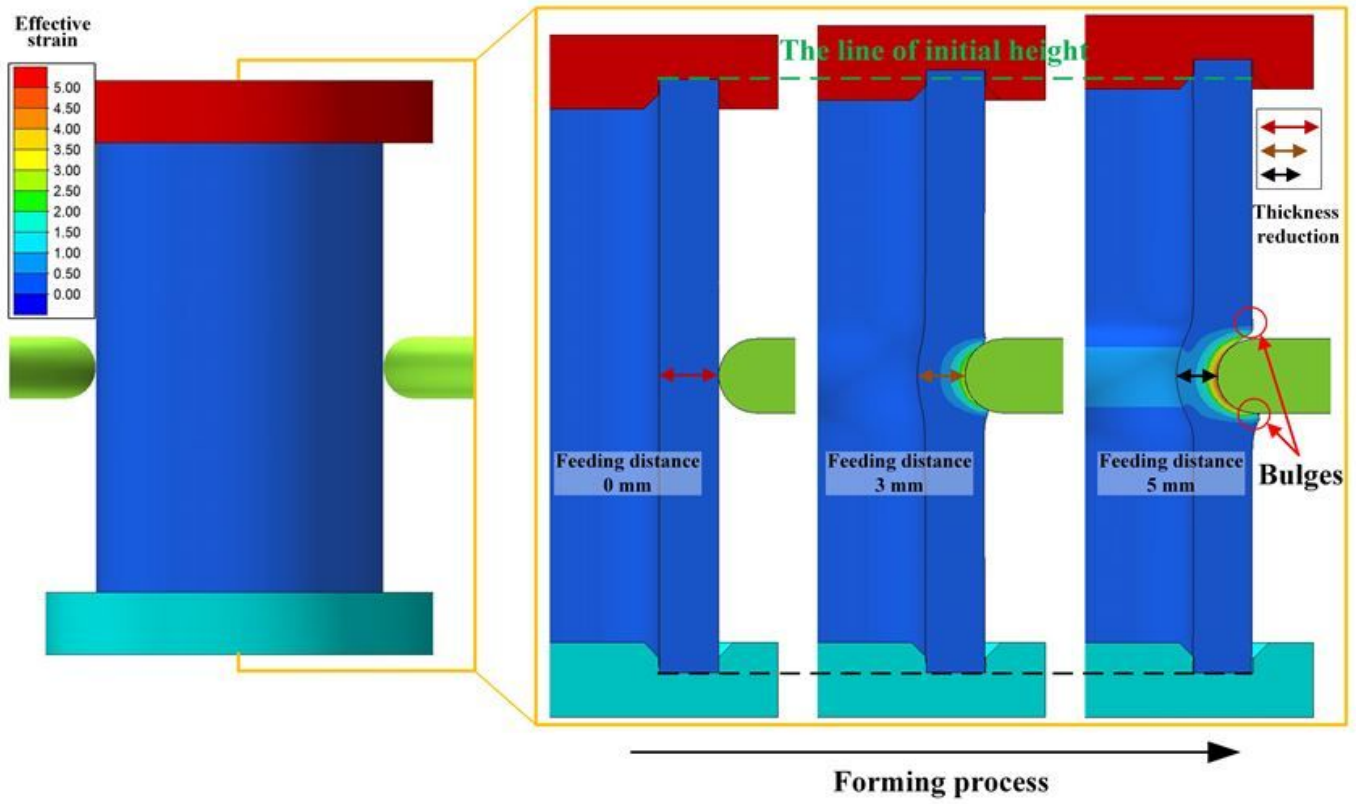
Figure 6

Typical forming process of DRSP (ξ = 0.06, η = 0.02, t0 = 8 mm)

The profile of the tube cross-section via simulations

The tube cross-section via experiments

Experiment

Experiment

Experiment

Experiment

Tube from No.4 test
$\xi = 0.06$, $\eta = 0.3$, $t_0 = 4mm$

Tube from No.8 test
$\xi = 0.14$, $\eta = 0.3$, $t_0 = 8mm$
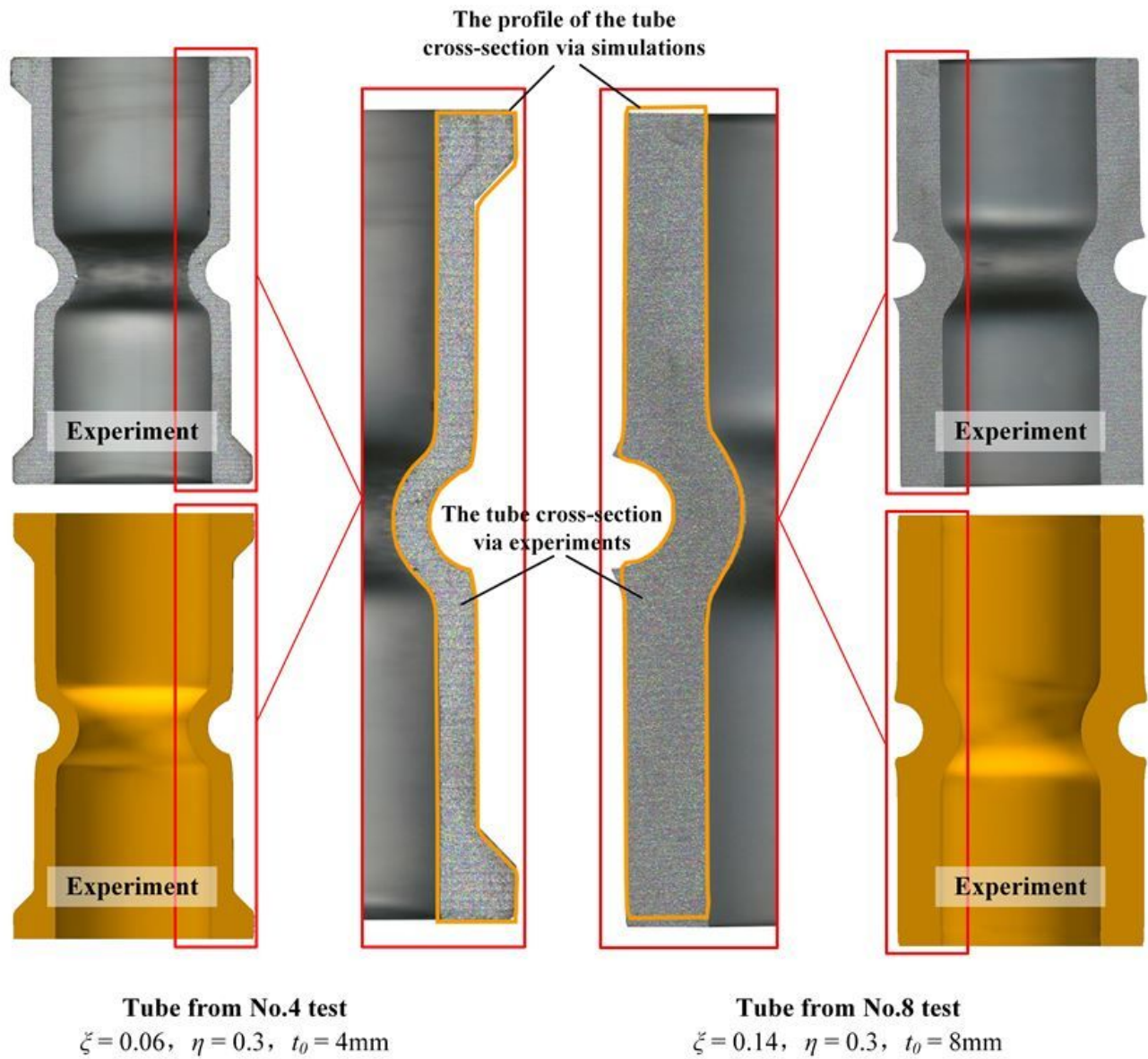
Figure 7

Comparison of shapes obtained by experiments and simulations
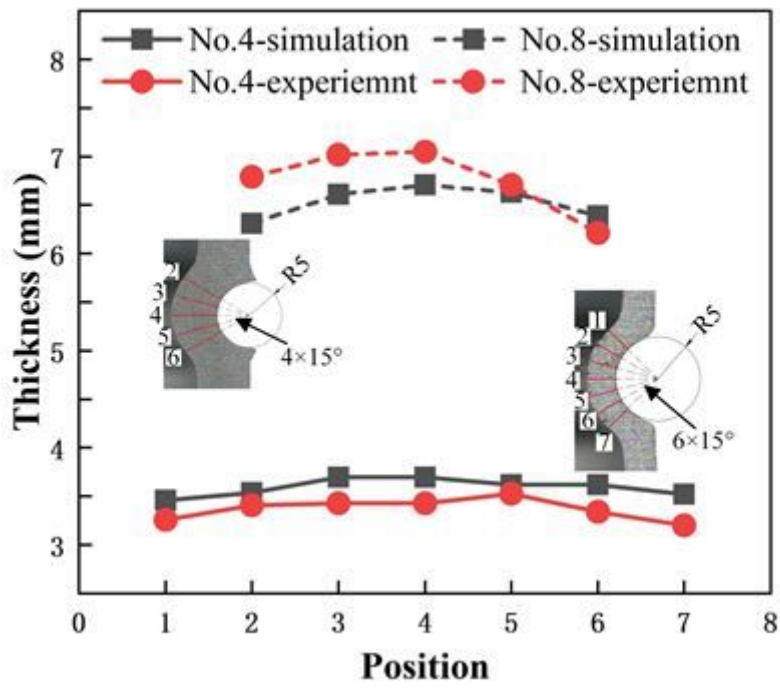
Figure 8

Comparison curves of groove thicknesses obtained from tests No. 4 and No. 8 by experiments and simulations
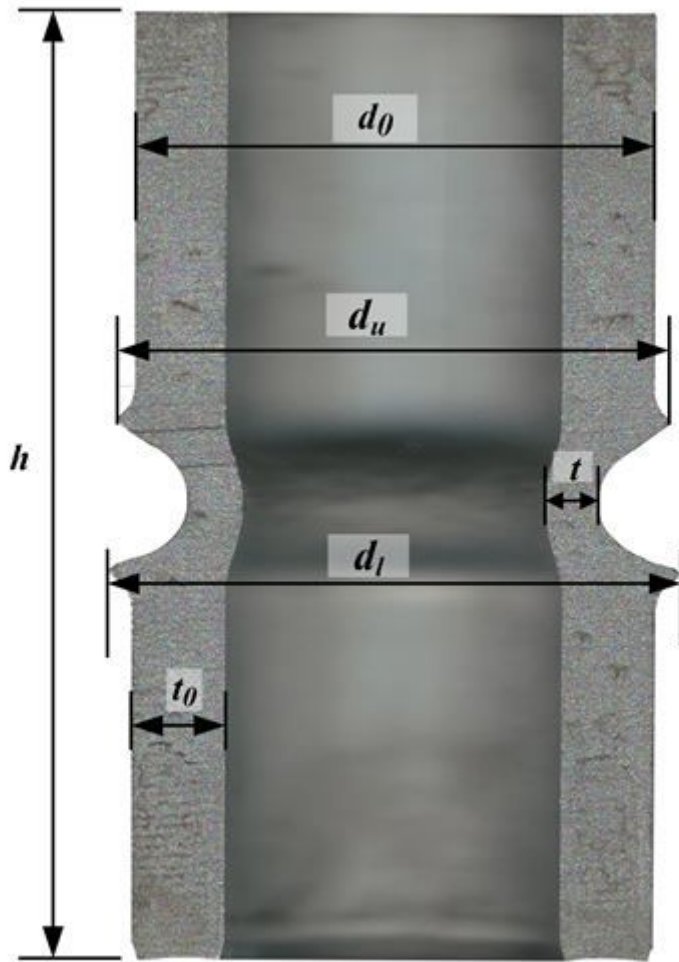
Figure 9

Schematic diagram of shape parameters
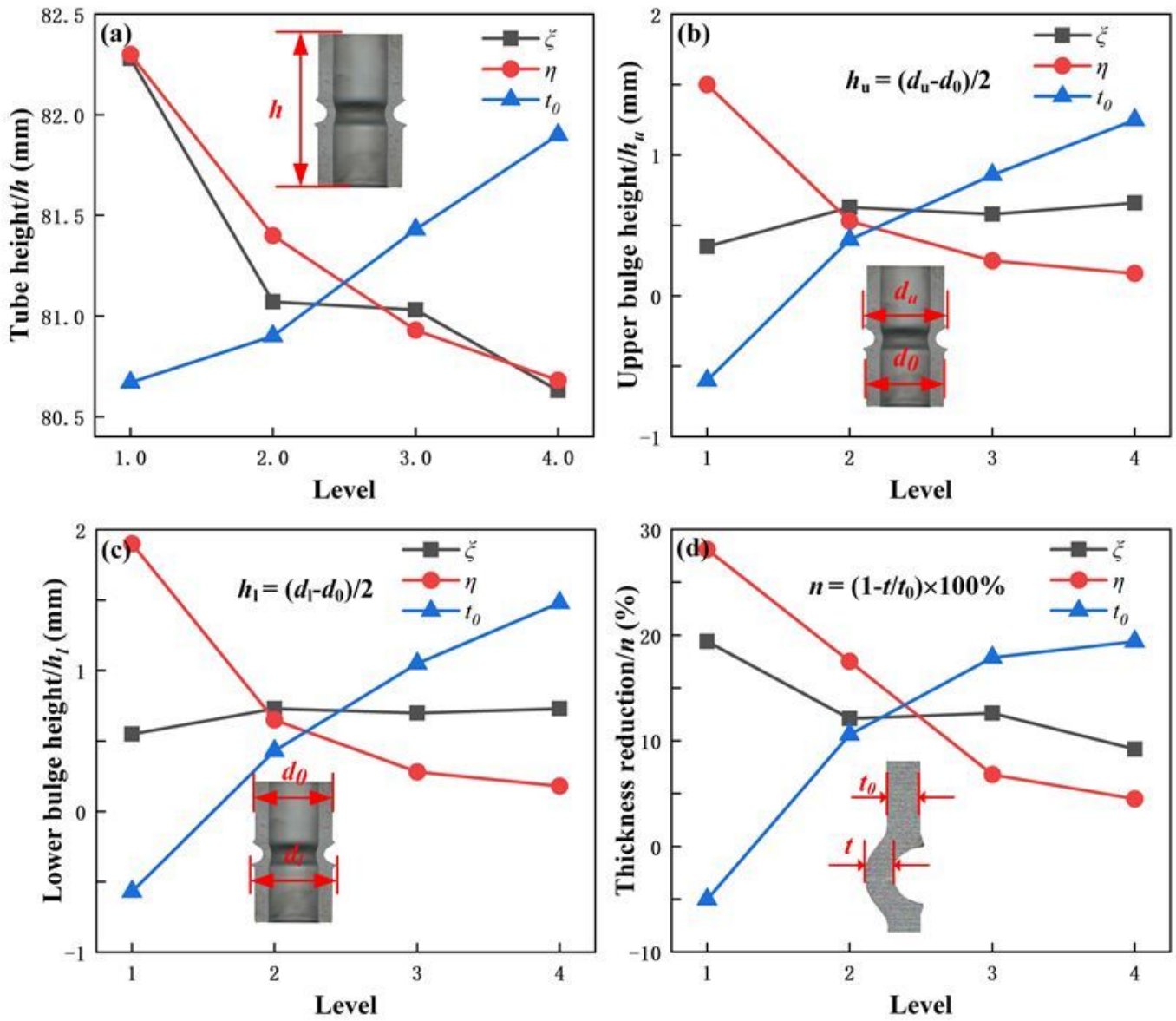
Figure 10

Effects of process parameters on measurement indexes according to range analysis
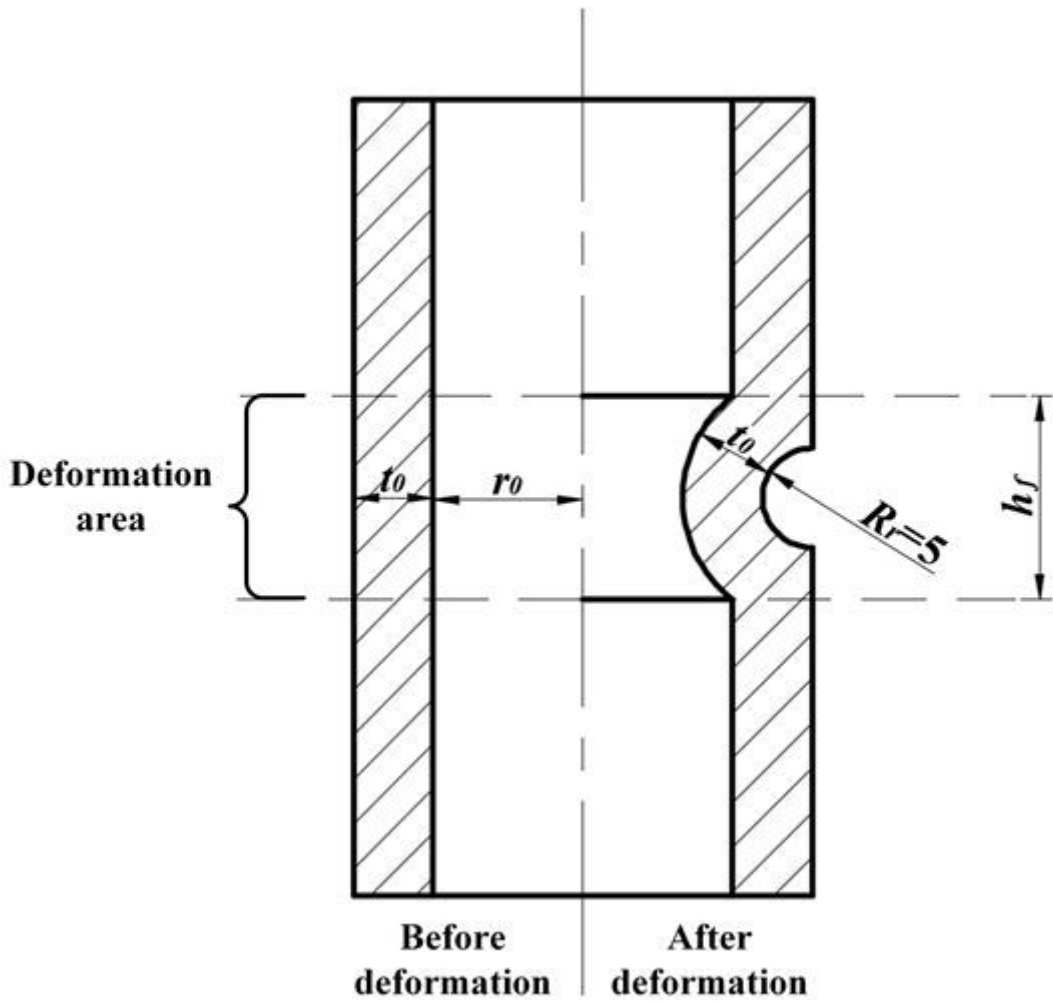
Figure 11

Change in deformation area before and after spinning, with assumption that wall thickness remains constant
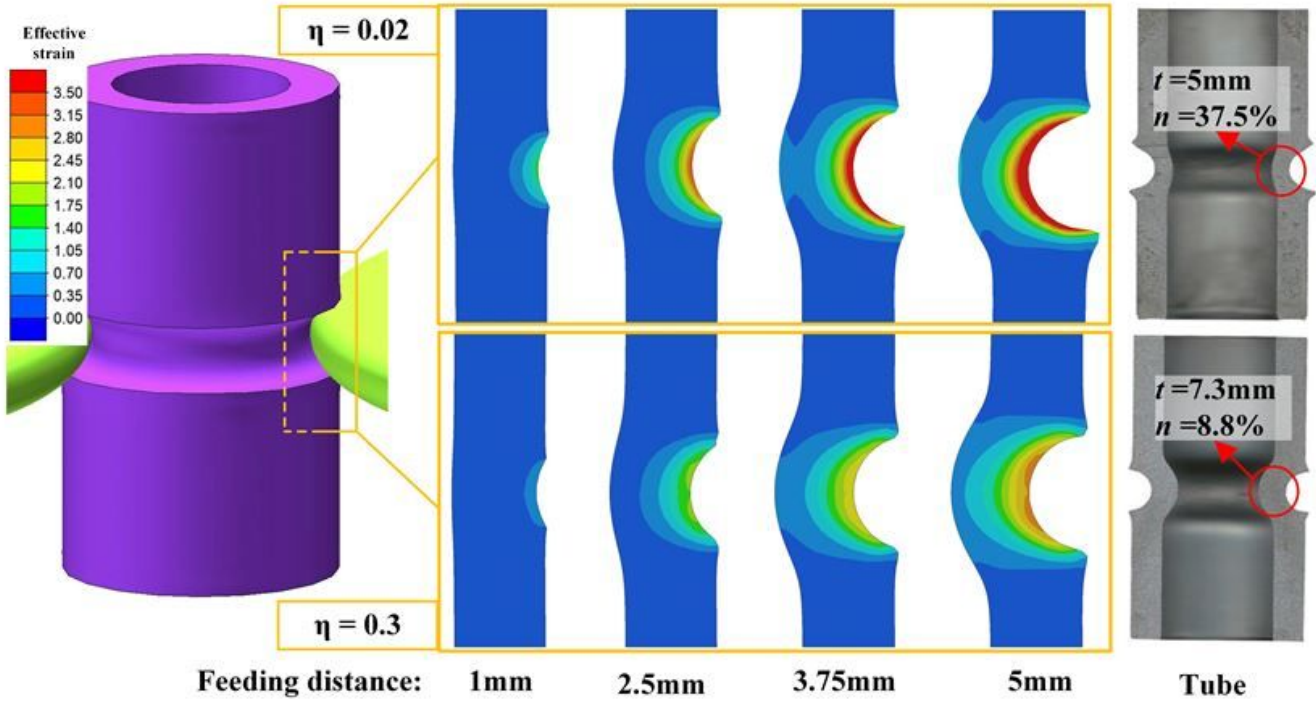
Figure 12

Strain distributions in deformation area at different feeding distances (t0 = 8 mm, ξ = 0.14, η = 0.02 and 0.30)
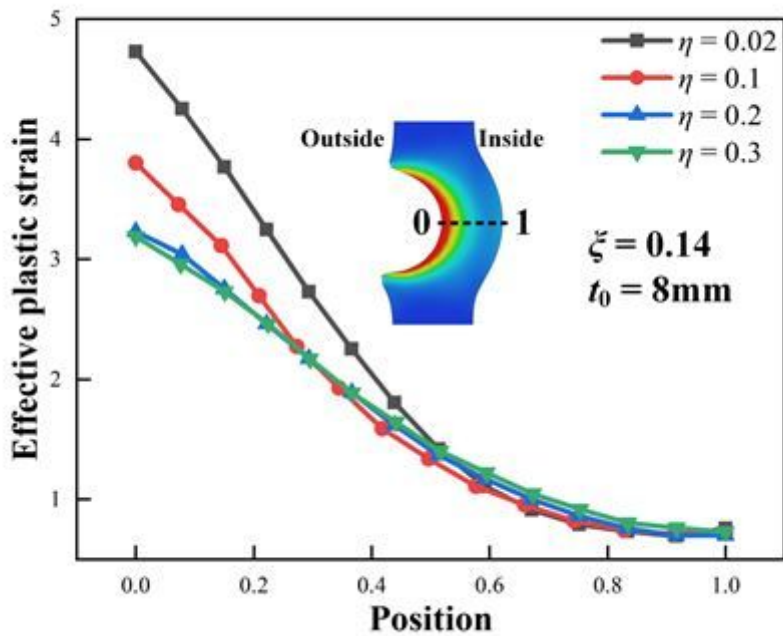
Figure 13

Strain distributions at middle of groove at different η values (ξ = 0.14, t0 = 8 mm)
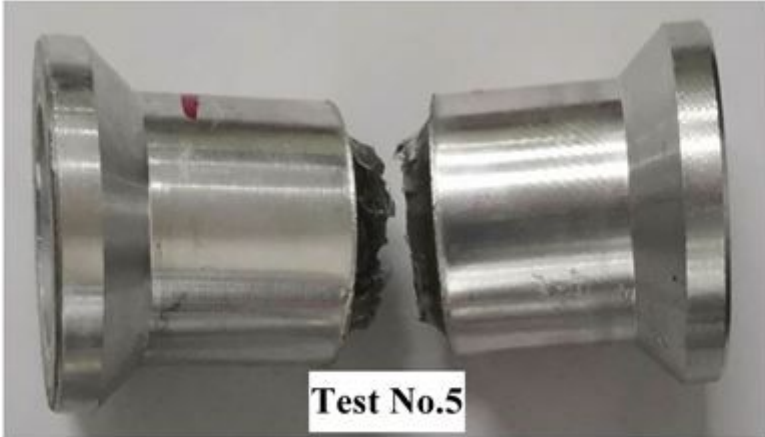
Figure 14

Tubes obtained by experiments in tests No. 2 and No. 5

$t = 5\text{mm}$
$n = 37.5\%$

$t_0 = 8\text{mm}$

$t = 3.4\text{mm}$
$n = 15\%$

$t_0 = 4\text{mm}$
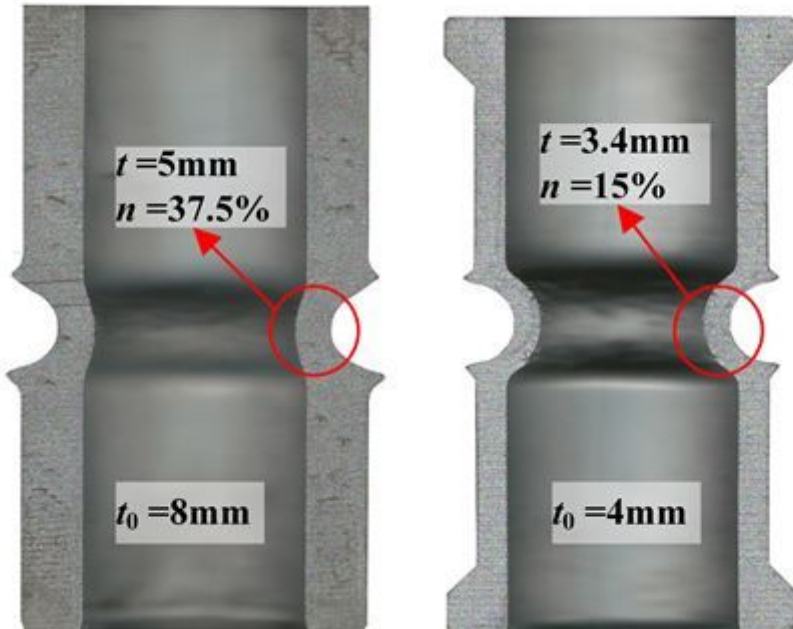
Figure 15

Axial profiles of tubes obtained by experiments with η = 0.02 and t0 = 4, 8 mm
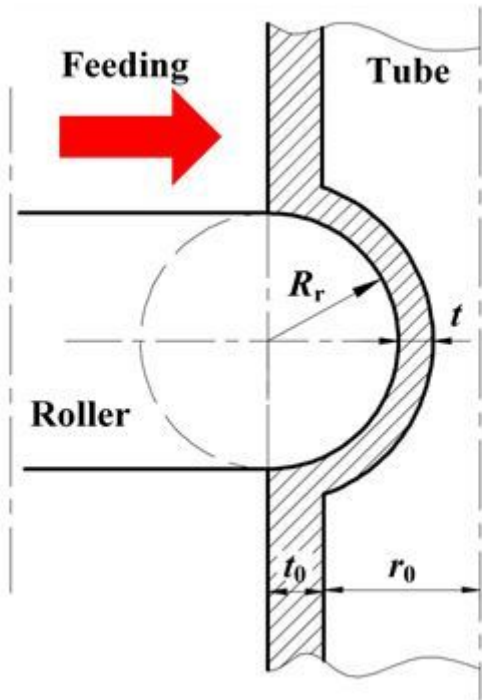
Figure 16

Axial profile schematic diagram of DRSP, with assumption that groove thickness was uniform
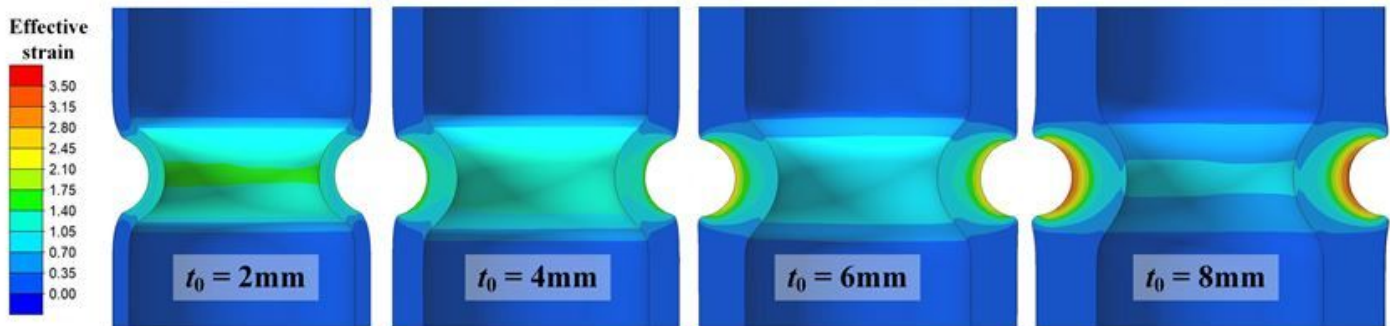
Figure 17

Strain distribution of the tubes with different t0 via simulations(ξ = 0.14, η = 0.2)
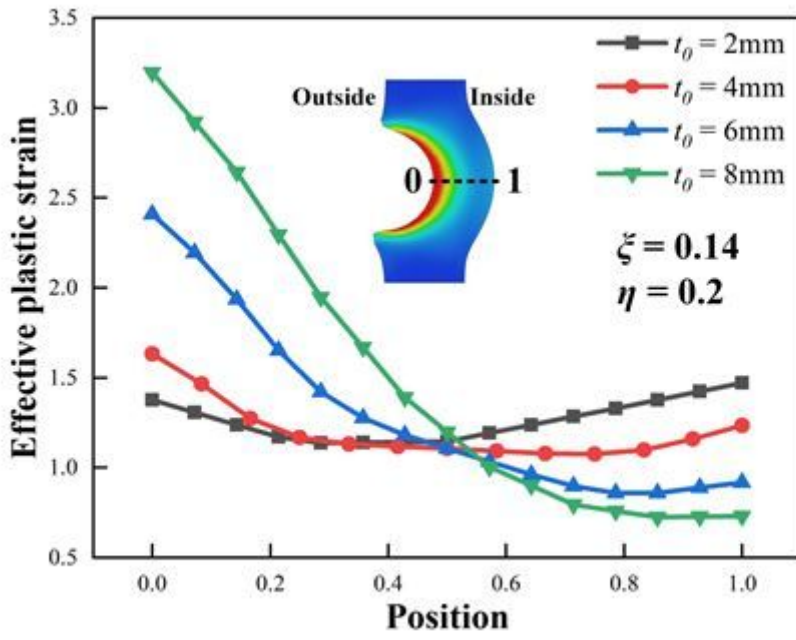
Figure 18

Strain distribution curves of grooves with different t0 via simulations ($\xi = 0.14$, $\eta = 0.2$)
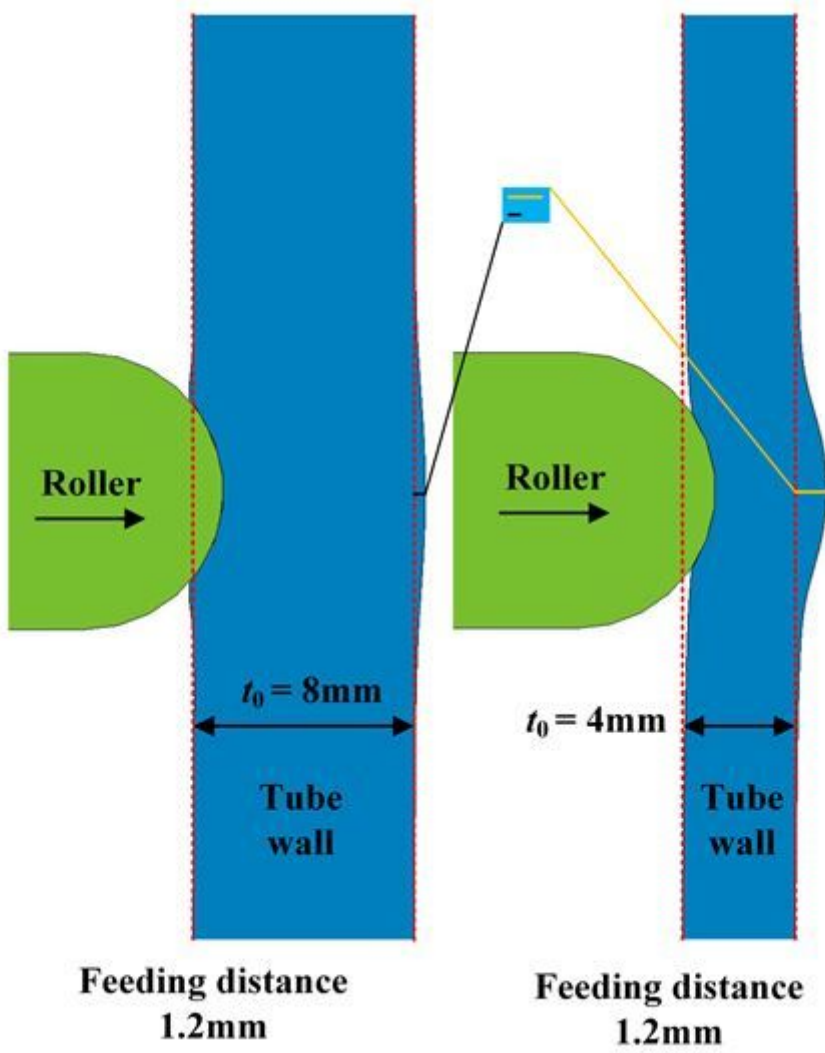
Figure 19

Deformations of grooves with different t0 values and feeding distance 1.2 mm ($\xi = 0.14$, $\eta = 0.2$, $t0 = 8, 4$ mm)
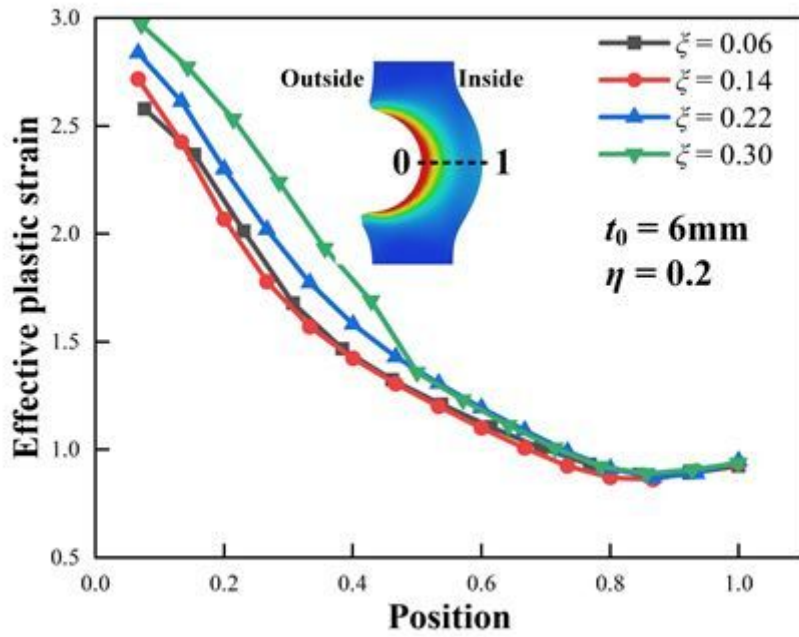
Figure 20

Strain distributions of grooves with different ξ values (η = 0.2, t0 = 6 mm)
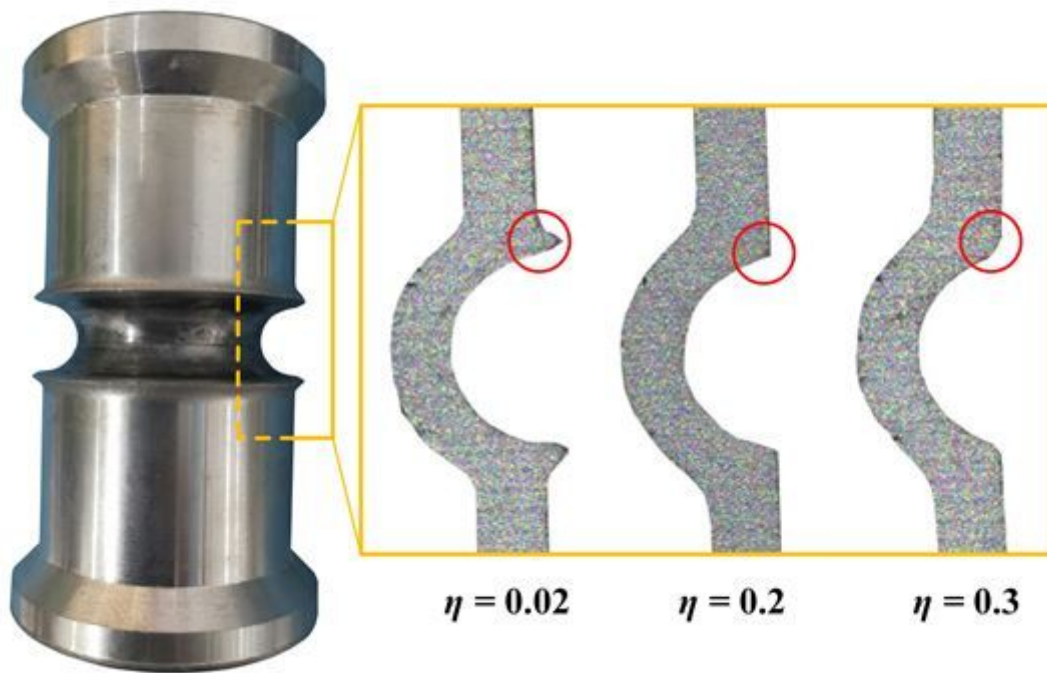
Figure 21

Upper/lower bulges formed in tubes during experiments with different η values (t0 = 4 mm, ξ = 0.14)
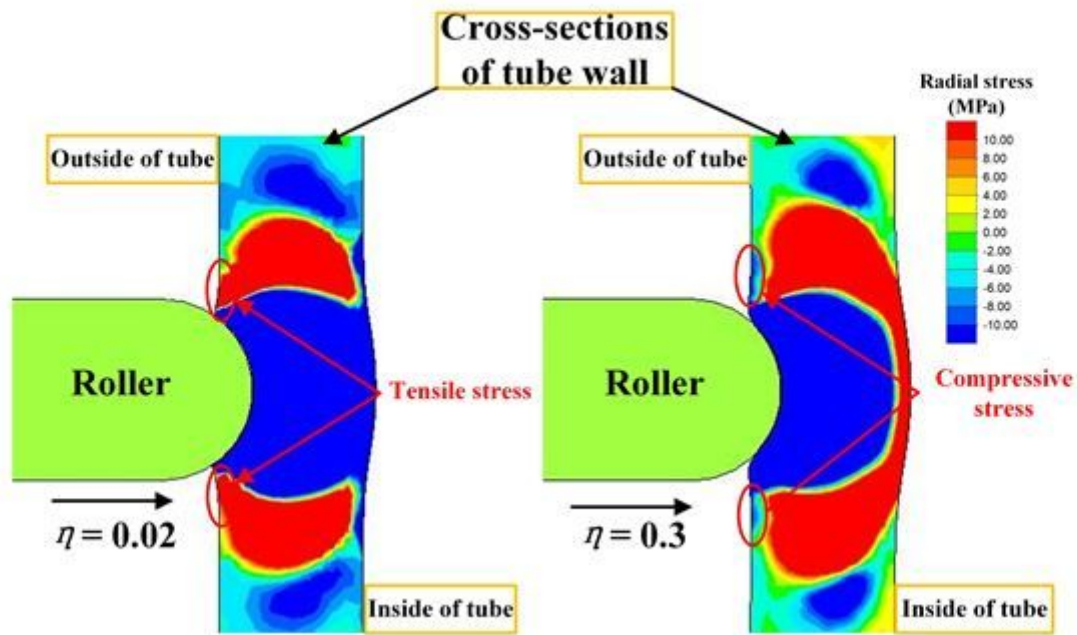
Figure 22

Radial stress distributions of deformation zones at different η values and feeding distance of 3 mm (t0 = 8 mm, ξ = 0.14)
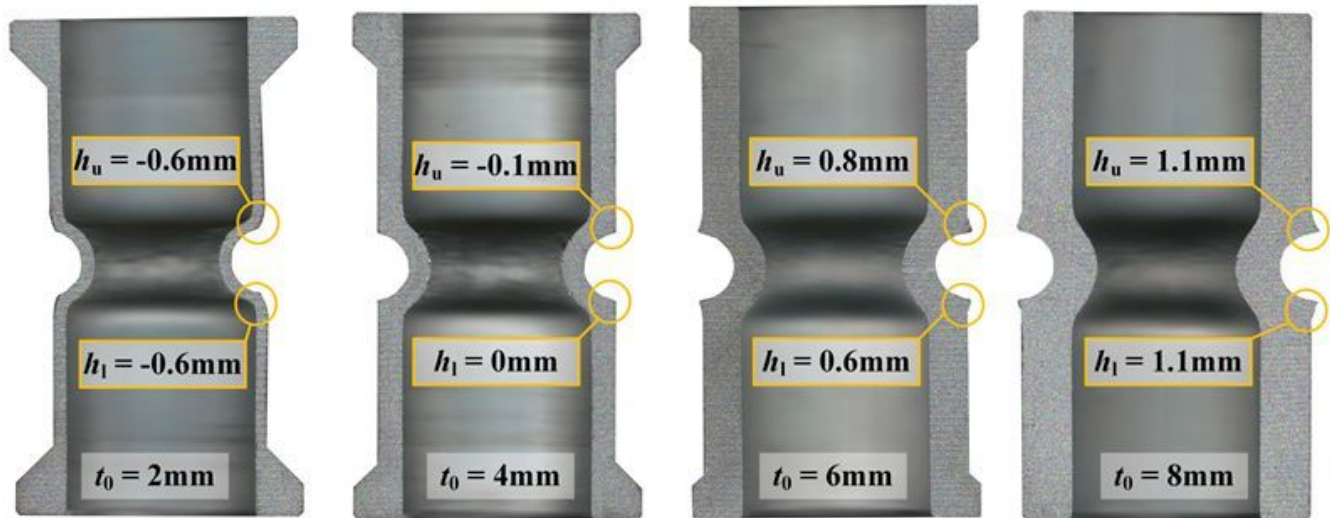

Figure 23

Upper/lower bulges formed in tubes during experiments with different t0 values (η = 0.2, ξ = 0.14)
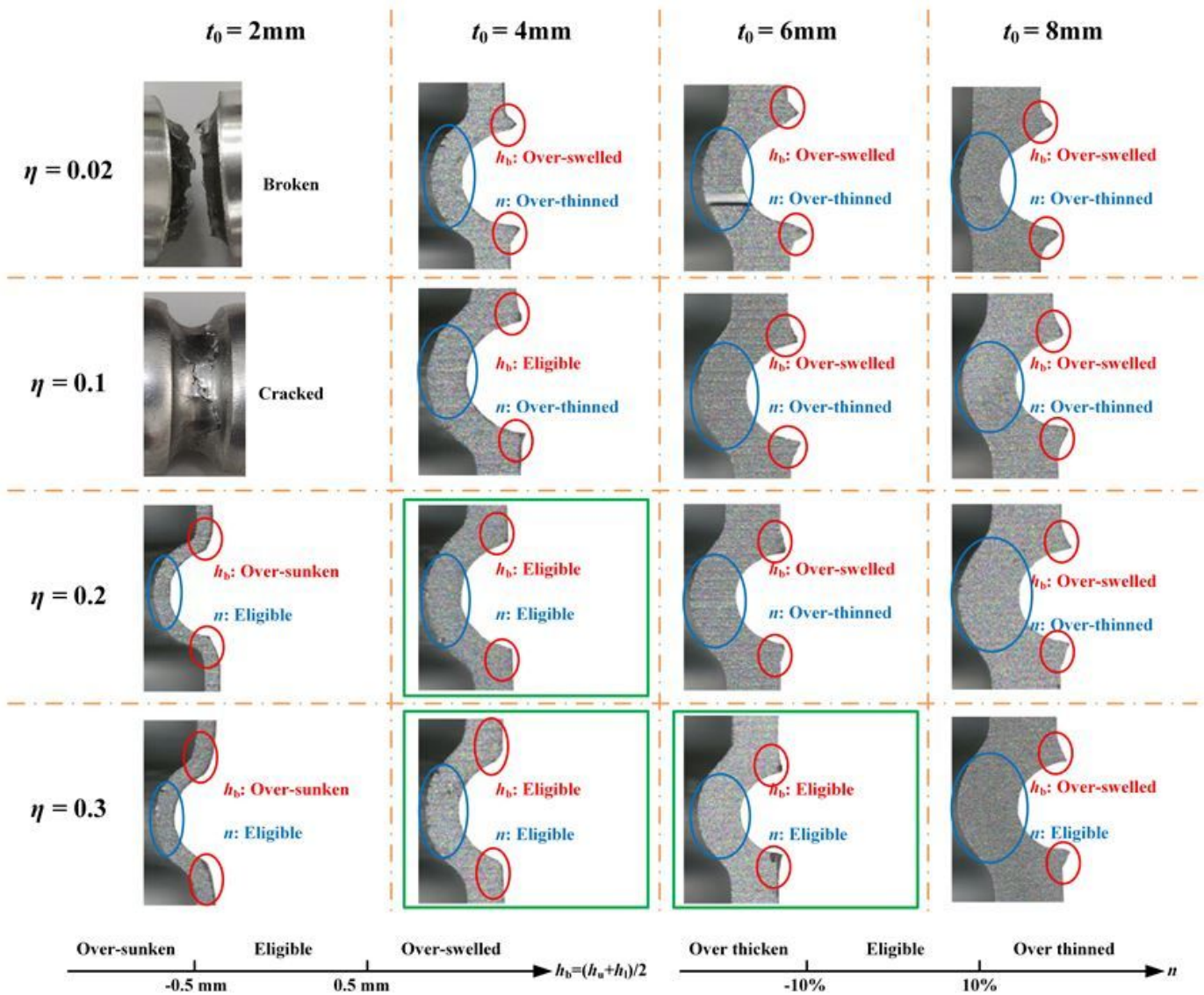
Figure 24

The forming qualities with different t0 and η values obtained by experiments

Supplementary Files

This is a list of supplementary files associated with this preprint. Click to download.

- AppendixA.docx